Quaternary Science Reviews 369 (2025) 109567

Contents lists available at ScienceDirect

Quaternary Science Reviews

journal homepage: www.elsevier.com/locate/quascirev

Mechanisms driving the global tropical response to a weakened AMOC during Heinrich Stadial 1

A.E. Lawman [a,*], C. Sun [b], X. Wu [c], T. Sun [d], N. Piatrunia [e], K. Gomez [e], M. Kageyama [f], U. Merkel [g], M. Prange [g], B. Otto-Bliesner [h], X. Zhang [i], P. DiNezio [j], T. Shanahan [e]

[a] Environmental Studies and Science Program, Colorado College, United States of America
[b] Department of Earth and Planetary Sciences, University of California Davis, United States of America
[c] Department of Sustainable Earth Systems Sciences, The University of Texas at Dallas, United States of America
[d] Environmental Defense Fund, United States of America
[e] Department of Earth and Planetary Sciences, Jackson School of Geosciences, The University of Texas at Austin, United States of America
[f] Laboratoire des Sciences du Climat et de l'Environnement/Institut Pierre-Simon Laplace, Universit'e Paris-Saclay, France
[g] MARUM – Center for Marine Environmental Sciences, University of Bremen, Germany
[h] Climate and Global Dynamics Laboratory, NSF National Center for Atmospheric Research, United States of America
[i] British Antarctic Survey, United Kingdom
[j] Department of Atmospheric and Oceanic Sciences, University of Colorado Boulder, United States of America

ARTICLE INFO

Handling Editor: Qiuzhen Yin

Dataset link: https://doi.org/10.5281/zenodo.16903147, https://github.com/lawmana/Lawman_etal_2025_QSR/

Keywords:
Paleoclimatology
Tropical hydroclimate
Abrupt climate change
Atmospheric circulation
Paleoclimate proxies
Global climate models

ABSTRACT

Heinrich Stadial 1 (HS1; ~17.5-15 thousand years before present) was characterized by a weakening of the Atlantic Meridional Overturning Circulation (AMOC) that resulted in large hydroclimate changes across the global tropics. Here we investigate the mechanisms driving tropical rainfall changes by comparing an ensemble of numerical simulations against paleoclimate proxy records spanning the global tropics. Our multi-model ensemble and synthesis of 154 hydroclimate records both show drier conditions north of the equator and wetter conditions south of the equator - a pattern broadly consistent with a meridional mean shift in tropical rain belts. However, changes in rainfall outside of the Atlantic and in monsoonal regions require more complex mechanisms to explain the proxy-inferred patterns. Cooling of the tropical North Atlantic emerges as the key link connecting AMOC weakening and the tropical hydroclimate response. Mechanisms involving tropical North Atlantic cooling are essential for propagating the North Atlantic climate signals to remote regions such as West Africa, the Indian Ocean, and the Andes. Simulations and the proxy synthesis show globally consistent response patterns except for the Maritime Continent. Reconciling these differences will require the separation of different proxy types and improved proxy system modeling for this region.

Plain language summary

The Atlantic Meridional Overturning Circulation (AMOC) is a system of currents that move heat from the southern to the northern hemispheres and its variations modulate global climate. Future changes in the strength of this system of currents have the potential to impact rainfall patterns worldwide, but the regional details of this response remain unclear. To understand how the global tropics respond to an abrupt decrease in AMOC strength, this study compares simulations from climate models to records of past rainfall changes from natural climate archives. We find that a weaker AMOC cools the high latitude Northern Hemisphere and is then communicated to the tropics via a series of mechanisms. The models that simulate cooling of the tropical North Atlantic agree best with the rainfall patterns inferred from the records.

1. Introduction

Changes in the strength of the Atlantic Meridional Overturning Circulation (AMOC) – the system of currents that transport heat northward across the equator – have the potential to alter rainfall patterns across the tropics via redistribution of heat between the hemispheres (Buckley and Marshall, 2016). Model projections indicate that this system of currents will likely weaken in response to anthropogenic warming, becoming a key driver of temperature and rainfall changes across the global tropics (Pörtner et al., 2022; Bellomo et al., 2021). However, model

* Corresponding author.
E-mail address: alawman@coloradocollege.edu (A.E. Lawman).

https://doi.org/10.1016/j.quascirev.2025.109567
Received 16 January 2025; Received in revised form 15 July 2025; Accepted 2 August 2025

discrepancies exist and the physical mechanisms that link changes in AMOC to the global tropics represent a major uncertainty (Kent et al., 2015; Bellomo et al., 2021; Pörtner et al., 2022). Recent trends in observed AMOC strength are small and hard to detect, making it difficult to determine the mechanisms based on observations alone (Bellomo et al., 2021; Kilbourne et al., 2022). Climate changes in the geological past provide an alternative opportunity to clarify the connection between AMOC strength and the global tropical hydroclimate response.

Over the past decades, many paleoclimate records have been produced showing evidence for millennial-scale fluctuations in rainfall concurrent with changes in the strength of AMOC (Hughen et al., 1996; Peterson, 2000; Hendy et al., 2002; Stager et al., 2011; Deplazes et al., 2013; Wang et al., 2004; McManus et al., 2004; Lippold et al., 2009; Böhm et al., 2015). Heinrich Stadial 1 (HS1), ~17.5-15 thousand years before present (kiloannum, ka), is a recent interval with clear evidence of an AMOC reduction and widespread temperature and hydroclimate changes (Stanford et al., 2011; Wang et al., 2001; McManus et al., 2004; Stager et al., 2011). Paleoclimate proxy records from HS1 show rainfall changes in regions remote from the North Atlantic. These changes include wetter conditions over South America, and drier conditions over East Asia, the Maritime Continent, and the Indian Ocean, suggesting regionally coherent rainfall responses to reduced AMOC across the global tropics (Bradley and Diaz, 2021; Stager et al., 2011; Hughen et al., 1996; Peterson, 2000; Wang et al., 2004, 2006, 2001, 2008; Partin et al., 2007). However, previous syntheses had a limited spatial scope (Du et al., 2023; Oster et al., 2023) or defined changes relative to the modern climate (Stager et al., 2011), thus hindering the comparison against simulations of AMOC weakening and the study of mechanisms.

There are several mechanisms through which a reduction in AMOC strength could influence rainfall patterns across the tropics. An important mechanism involves a southward shift in the Intertropical Convergence Zone (ITCZ), the ascending branch of the Hadley circulation, where surface winds converge and intense rainfall occurs. To compensate for reduced northward ocean heat transport due to a weaker AMOC, the ITCZ shifts southward and transports more energy via the atmosphere from the tropics to higher northern latitudes (Kang et al., 2008; Clement and Peterson, 2008; Swingedouw et al., 2009; Kageyama et al., 2013; Marzin et al., 2013; Ma et al., 2024). Climate models and proxy data show patterns that are broadly consistent with a southward ITCZ shift expected from the energetic argument outlined above (Vellinga and Wood, 2002; Zhang and Delworth, 2005; Kang et al., 2008; Clement and Peterson, 2008; Marshall et al., 2013; Schneider et al., 2014). That said, some proxy records and models show departures from this response, for instance over the continents and in monsoonal regions (McGee et al., 2014, 2018; Stager et al., 2011), highlighting that a zonally symmetric ITCZ shift cannot fully explain the simulated and proxy inferred regional rainfall changes. Alternative mechanisms have been proposed for specific regions (Clement and Peterson, 2008; Du et al., 2023), but further research is needed to comprehensively understand the impact of an AMOC reduction on rainfall patterns across the entire global tropics.

To better understand the mechanisms that link tropical rainfall changes to weakened AMOC during HS1, here we synthesize and select a network of 154 rainfall-sensitive proxy records that span the global tropics to infer patterns of hydroclimate change. We compare the proxy-inferred patterns against an ensemble of 18 numerical experiments that simulate LGM and HS1 climates, performed with 8 different climate models. First we characterize the patterns of inferred and simulated tropical rainfall change. Then for regions where the proxy records exhibit spatially coherent responses, we use the simulations to explore both dynamic and thermodynamic mechanisms linking weaker AMOC to the hydroclimate changes. We conclude by emphasizing the important role of tropical Atlantic temperature patterns in generating zonally asymmetric rainfall responses that best agree with the patterns inferred from the proxy records.

2. Methods

2.1. Multi-proxy synthesis of tropical hydroclimate changes during HS1

We used published paleoclimate records to reconstruct patterns of hydroclimate change during HS1. The records were selected following a series of criteria allowing the isolation of changes associated with the reductions in AMOC strength during this interval. This is particularly important for the comparison of reconstructed changes against the simulated changes. The selection criteria were applied to published rainfall-sensitive proxy records spanning the HS1 interval as follows:

1. **Global tropical domain:** The study site is located between 25°S and 25°N. These boundaries were extended to 30°N in northern Mexico and 35°N along the coast of North Africa to include sites potentially sensitive to changes in monsoon systems. Several stalagmite records from China north of 25°N were excluded because they may reflect non-local effects and it is unclear if they should be compared against local rainfall changes (Pausata et al., 2011).
2. **Rainfall-sensitive proxy:** The climate proxy is sensitive to changes in rainfall based on well-established relationships between the proxy measurements and precipitation or aridity. The types of proxies are further described in the paragraph following the selection criteria.
3. **Sufficiently long record to identify baseline climate:** The proxy record extends back to the Last Glacial Maximum (LGM: 21–19 ka) or demonstrates a clear deglacial trend, which provides a reference interval to determine the observed rainfall changes during HS1. The use of an LGM reference state was chosen for consistency with the simulations (Section 2.2). The LGM is also closer to the mean climate state prior to HS1 than the pre-industrial.
4. **Sufficient temporal resolution to resolve HS1:** The record has at least ~500-year resolution during the ~17.5–15 ka interval for HS1. The Nyquist sampling theorem requires that a frequency of at least one sample per 1000 years is needed in order to correctly capture the signal of a 2000-year event. Considering potential age uncertainties, analytical errors, and varying signal-to-noise ratios, we double the temporal resolution in our data selection criteria, requiring 5 data points between 17.5–15 ka. This approach allows for unambiguous identification of HS1 changes, improving our confidence in the regional signals of hydroclimate change during HS1.

The publicly available synthesis (DiNezio et al., 2025a) includes records based on marine and terrestrial stable isotopes, aridity, and vegetation proxies (Fig. 1a, symbols). The stable isotope records include hydrogen isotope ratios from leaf waxes (δD_{wax}) from both marine and lake sediments, oxygen isotope ratios from cave speleothems ($\delta^{18}O_{calcite}$), and $\delta^{18}O$ records reconstructed from surface dwelling foraminifera. Foraminiferal $\delta^{18}O$ is a function of both temperature and the $\delta^{18}O$ of seawater/salinity (Ravelo and Hillaire-Marcel, 2007). Our interpretation of hydroclimate change is based on available $\delta^{18}O$ of seawater records where $\delta^{18}O$ was corrected by the original authors using the accompanying Mg/Ca temperature data from the same core to remove the temperature effect. We interpret the $\delta^{18}O$ of seawater as a proxy for rainfall, but note that this proxy is also sensitive to changes in evaporation, ocean circulation (advection) and runoff (Ravelo and Hillaire-Marcel, 2007). The synthesis also includes non-isotope aridity records, including dust fluxes, terrigenous sediment discharge (e.g. titanium or aluminum fluxes), and high-resolution lake level reconstructions. Lastly, vegetation-related proxy records include carbon isotope ratios ($\delta^{13}C$) and pollen records from marine and lake sediments. Many of the records are publicly available via the NOAA World Data Service for Paleoclimatology (https://www.ncdc.noaa.gov/data-

access/paleoclimatology-data/datasets) or the PANGAEA Data Publisher for Earth and Environmental Science (https://www.pangaea.de) repositories.

The changes in each selected record were classified as wetter, drier, or unchanged during HS1 relative to the LGM or the deglacial reference interval (Fig. 1a, symbol color). The interpretations were largely consistent with the original studies, but were updated accordingly to reflect our choice of an LGM baseline. This allowed direct comparison with the responses to AMOC weakening simulated in our multi-model ensemble (Section 2.2). While evaporation and other processes may influence some proxies, the direction of change (i.e., wet, dry, or unchanged) is typically driven by precipitation. Moreover, because precipitation and evaporation often vary coherently, these additional influences are unlikely to affect our categorical interpretations.

2.2. Multi-model ensemble of freshwater hosing simulations

We explored mechanisms driving tropical climate changes in response to weakened AMOC using a multi-model ensemble of climate model simulations. In all simulations, the strength of the AMOC was reduced by applying a freshwater flux over the North Atlantic to reduce surface salinity and suppress wintertime convection. These so-called "freshwater hosing" simulations are characterized by a weakening of the sinking branch of the AMOC, producing cooling over the Northern Hemisphere and widespread changes in global climate (Manabe and Stouffer, 1995; Stouffer et al., 2006; Clement and Peterson, 2008; Kageyama et al., 2010, 2013; Ma et al., 2024). Our ensemble consists of 18 simulations generated using 8 different coupled global climate models with different rates and locations of freshwater forcing to produce a range of responses in the AMOC strength (Table 1). The size of our ensemble allowed us to investigate model-dependencies in the response and identify consistent mechanisms that explain the patterns inferred from the proxy data (Section 2.1).

All freshwater hosing simulations were performed under glacial conditions, facilitating the comparison with the proxy records for HS1 (Section 2.1). Our ensemble is an "ensemble of opportunity" with no common hosing protocol, but the simulations were designed similarly such that they can be compared. It consists of the 9 simulations analyzed by Kageyama et al. (2013) and 9 recently published simulations, performed with modified freshwater forcing scenarios or newer model versions (Table 1) (Singarayer and Valdes, 2010; Otto-Bliesner and Brady, 2010; Merkel et al., 2010; Kageyama et al., 2009; Liu et al., 2009; Kageyama et al., 2012; Erokhina et al., 2017; Campos et al., 2019; Bakker et al., 2020; Zhang et al., 2013; Chikamoto et al., 2012; He et al., 2021; DiNezio et al., 2025b). Most of the simulations in the ensemble followed the PMIP2 protocol for the LGM (Braconnot et al., 2007) as the control simulation, with the exception of the HadCM3 simulations that used a 24 ka reference state (Singarayer and Valdes, 2010).

The ensemble also includes two transient simulations (CCSM3-TraCE-MWF and CESM1-iTraCE-MWF). CCSM3-TraCE-MWF is a single-forcing simulation in which transient meltwater forcing was applied, whereas orbital insolation, ice sheet, and greenhouse gases were held constant at LGM levels (He, 2011). The CESM1 iTraCE project (He et al., 2021) is a set of transient simulations where climate forcings were applied additively to the isotope-enabled Community Earth System Model version 1.3 (iCESM1.3). The full forcing simulation has time-varying ice sheet, greenhouse gases, insolation, and meltwater forcing. To isolate the climate responses to meltwater forcing during 17–15 ka, we calculated the difference between the full forcing simulation and the factorized simulation with only ice sheet, greenhouse gas, and insolation forcing. The 18 control simulations have a wide range of AMOC strengths, ranging from 8.4 to 26.8 sverdrup (Sv, 1Sv = 10^6 m^3/s), allowing us to explore the sensitivity of the response with respect to the initial AMOC state.

The reductions in AMOC strength were induced by applying a negative salinity flux (*i.e.*, a positive freshwater flux) in different regions such as the North Atlantic (50°–70°N), the Greenland–Iceland–Norwegian Seas (north of approximately 65°N), or the Ruddiman Belt in the North Atlantic (40°–50°N) (Table 1). Most simulations used a constant flux ranging from 0.1 Sv to 1.0 Sv. In CCSM3-TraCE-MWF, the freshwater flux was applied with gradually increasing amplitude from 19–17 ka and then held constant at 0.17 Sv from 17–15 ka. Similarly, in CESM1-iTraCE-MWF, the freshwater flux was increased from 19–17 ka and then held at a constant rate of 0.23 Sv from 17–15 ka (He et al., 2021). All hosing simulations produced an AMOC reduction in response to freshwater forcing (Table 1).

The response to the imposed freshwater flux (Figures S1 and 2) was defined as the difference between the respective freshwater hosing and the LGM control simulation (Figures S2 and S3). For each set of simulations, only annual mean surface air temperature and total precipitation were made available by all modeling centers. Surface air temperature changes over the ocean reflect changes in sea surface temperature (SST) well. We also analyzed monthly and seasonal mean precipitation, near-surface winds, and sea level pressure (SLP) changes from 4 simulations with full model output available (IPSL-CM5, CCSM3-1Sv-NA, CESM1-0.2Sv and CESM1-iTraCE-MWF; Figures S4-S5 and S10-S13). These diagnostics allowed for a more thorough understanding of seasonal moisture supply and rainfall dynamics in monsoon regions.

The simulations exhibited a wide range of temperature and hydroclimate responses to AMOC weakening. We first quantified the agreement between the simulated patterns of rainfall change and the patterns inferred from the proxy records. Then we used the model output to analyze the mechanisms driving these patterns in key regions across the global tropics. Following Kageyama et al. (2013), we use pattern correlation analysis to explore the relationships between simulated regional precipitation changes and large-scale temperature patterns (Section 3). Statistically significant correlations are reported using a two-tailed t-test at the 90% confidence interval unless otherwise noted.

2.3. Quantifying the model agreement with the proxy-inferred hydroclimate patterns

We quantified the agreement between the simulated and proxy-inferred patterns of hydroclimate change using the Cohen's (κ) statistic (Fig. 1b) (Cohen, 1960; DiNezio and Tierney, 2013). The simulated changes were first placed into the same wetter, drier, and unchanged categories as the network of proxy records (Section 2.1) using a range of wetter/drier thresholds from 0% to 60% (Fig. 1b) to explore the sensitivity of the model-data agreement. The agreement between the simulated and proxy-inferred patterns was then quantified using the Cohen's κ statistic, which is the observed fractional agreement (p_o) relative to the probability of random agreement (p_e) (DiNezio and Tierney, 2013):

$$\kappa = \frac{p_o - p_e}{1 - p_e} \quad (1)$$

The κ was determined for each simulation (Fig. 1b, x-axis) for the range of wetter/drier thresholds (Fig. 1b, y-axis). The highest Cohen's κ for each simulation (Fig. 1b) is reported in Table 1. A κ of 1 indicates perfect agreement between the simulation and the proxy-inferred patterns, whereas a κ of 0 indicates that the agreement could be expected entirely by chance. Thus, a value of 0 indicates complete disagreement between the simulated and proxy-inferred patterns. The Cohen's κ calculation was modified by a weighting matrix (Cohen, 1960; DiNezio and Tierney, 2013) so that a model was penalized for a total miss (e.g., the model is drier when the proxy records show wetter) to a greater degree than a near miss (e.g., the model is drier when the proxy records show unchanged).

Table 1
The ensemble of 18 freshwater hosing simulations and their model configuration (Section 2.2). The table provides the model resolution of the atmosphere and ocean components, the rate (Sv) and location of freshwater forcing, the magnitude of the AMOC reduction (Sv), the percent decrease in AMOC strength compared to the initial state, the tropical North Atlantic temperature change (°C), and the Cohen's κ indicating the model agreement with the proxy-inferred hydroclimate patterns (Section 2.3). W = weak AMOC in the LGM control simulation and S = strong AMOC in the LGM control simulation. Locations of the freshwater forcing: NA = North Atlantic (50–70°N), GIN = Greenland–Iceland–Norwegian Seas (north of 65°N), RB = Ruddiman Belt in the North Atlantic (40–50°N). The simulations are ordered based on the magnitude of tropical North Atlantic cooling over the domain (12°–22°N, 80°–40°W).

	Freshwater Hosing	Resolution		Freshwater forcing		AMOC reduction		TNA cooling	Highest	Reference
	Simulation	Atmosphere	Ocean	Rate (Sv)	Location	(Sv)	(% decrease)	(°C)	Cohen's κ	
Simulations with strong and moderate tropical North Atlantic cooling										
1	HadCM3-0.4Sv	3.75° x 2.5° L19	1.25°	0.4	NA	15.1	68	-5.4	0.42	*Singarayer and Valdes (2010)*
2	CCSM3-1Sv-NA	2.8° x 2.8° L26	1°	1	NA	12	80	-3.8	0.42	*Otto-Bliesner and Brady (2010)*
3	CESM1-0.2Sv	2.5° x 1.9° L30	1° L54	0.2	NA	14.9	81	-3.2	0.42	*DiNezio et al. (2025)*
4	CCSM3-0.2Sv-GIN-LR	3.75° x 3.75° L26	3° L25	0.2	GIN	6.6	65	-2.4	0.54	*Merkel et al. (2010)*
5	IPSL-CM4	3.75° x 2.5° L19	2° L31	0.1	NA	10	77	-2.2	0.48	*Kageyama et al. (2009)*
6	CCSM3-TraCE-MWF	3.75° x 3.75° L26	3° L25	0.17	NA	9.5	76	-2.2	0.57	*Liu et al. (2009)*
7	CESM1-iTraCE-MWF	2.5° x 1.9° L30	1° L60	0.23	NA	15	75	-2.2	0.53	*He et al. (2021)*
8	IPSL-CM5	3.75° x 1.8° L39	2° L31	0.1	NA	12.5	78	-1.7	0.50	*Kageyama et al. (2013)*
9	CCSM3-0.2Sv-GIN-HR	1.4° x 1.4° L26	1° L40	0.2	GIN	6	50	-1.6	0.41	*Campos et al. (2019); Erokhina et al. (2017)*
10	CESM1-0.15Sv	2.5° x 1.9° L30	1° L54	0.15	NA	10.5	57	-1.6	0.33	*DiNezio et al. (2025)*
Simulations with muted tropical North Atlantic cooling										
11	CCSM4-0.1Sv-RB	2.5° x 1.9° L26	1° L60	0.1	RB	15	75	-0.9	0.48	*Bakker et al. (2020)*
12	COSMOS-W	3.75° x 3.75° L19	3° x 1.8°	0.2	RB	17.9	95	-0.8	0.33	*Zhang et al. (2013)*
13	COSMOS-S	3.75° x 3.75° L19	3° x 1.8°	0.2	RB	23.9	89	-0.6	0.34	*Zhang et al. (2013)*
14	CCSM3-0.1Sv-NA	2.8° x 2.8° L26	1°	0.1	NA	6.2	40	-0.5	0.40	*Otto-Bliesner and Brady (2010)*
15	MIROC-W	2.8° x 2.8° L20	1.4°	0.1	NA	5.4	64	-0.4	0.31	*Chikamoto et al. (2012)*
16	HadCM3-0.1Sv	3.75° x 2.5° L19	1.25°	0.1	NA	4.5	19	-0.3	0.24	*Singarayer and Valdes (2010)*
17	CESM1-0.1Sv	2.5° x 1.9° L30	1° L54	0.1	NA	4.7	25	-0.3	0.07	*DiNezio et al. (2025)*
18	MIROC-S	2.8° x 2.8° L20	1.4°	0.1	NA	16	84	0.0	0.22	*Chikamoto et al. (2012)*

3. Results

Our synthesis of hydroclimate changes during HS1 reveals coherent patterns in many regions across the global tropics. The proxy-inferred changes are broadly characterized as drier conditions in the northern tropics and wetter conditions in the southern tropics consistent with a southward shift of the ITCZ (Fig. 1a). Several spatially coherent regional rainfall patterns can be identified. For example, drier conditions over coastal West Africa, northeastern Africa, the Indian subcontinent, and wetter conditions over the tropical Andes, northeastern Brazil, southeastern Africa, and northern Australia (Fig. 1a). The proxy synthesis also shows several transitional zones with no rainfall responses (e.g., eastern Africa and coastal southwestern Africa).

The simulated temperature (Figure S1) and precipitation (Fig. 2) responses in the 18-member freshwater hosing ensemble show several common patterns. All the freshwater hosing simulations show pronounced cooling of the high-latitude North Atlantic (Figure S1). Over two-thirds of the simulations show Southern Hemisphere warming with varying spatial patterns and magnitudes. Inter-model temperature agreement is poorer in the Southern Hemisphere compared to the Northern Hemisphere, particularly in regions outside of the Atlantic (Figure S1). Cooling of the tropical North Atlantic (12°–22°N, 80°–40°W) is another feature of inter-model differences (Figures S1 and S7). We classify the simulations with an average temperature change less than −1 °C as the "strong and moderate cooling" group (Fig. 3a), while those with changes greater than −1 °C fall into the "muted cooling" group (Fig. 3c).

The simulated tropical rainfall response patterns (Fig. 2) are also broadly consistent with the proxy-inferred patterns during HS1 (Fig. 1a). For example, all freshwater hosing simulations show drier conditions across the northwestern coast of Africa and the Indian subcontinent, suggesting a direct connection with AMOC weakening and high-latitude cooling (Fig. 1c). Most of the simulations show wetter conditions in southern Africa and northeastern Brazil. The simulated rainfall patterns are the least consistent in East Asia and the Maritime Continent, where many of the simulations disagree on the sign of the rainfall change (Figs. 1c and 2). In the subset of simulations with both precipitation and evaporation available, we confirm that precipitation dominates the simulated changes in precipitation minus evaporation (P-E; Figure S6). Precipitation and P-E change with the same sign across most of the tropics, further demonstrating that the categorical interpretations of the proxy records (wetter, drier, unchanged) would be consistent for either P or P-E (Figure S6).

While drier northern tropics and wetter southern tropics are consistent with a southward ITCZ shift, the freshwater hosing simulations

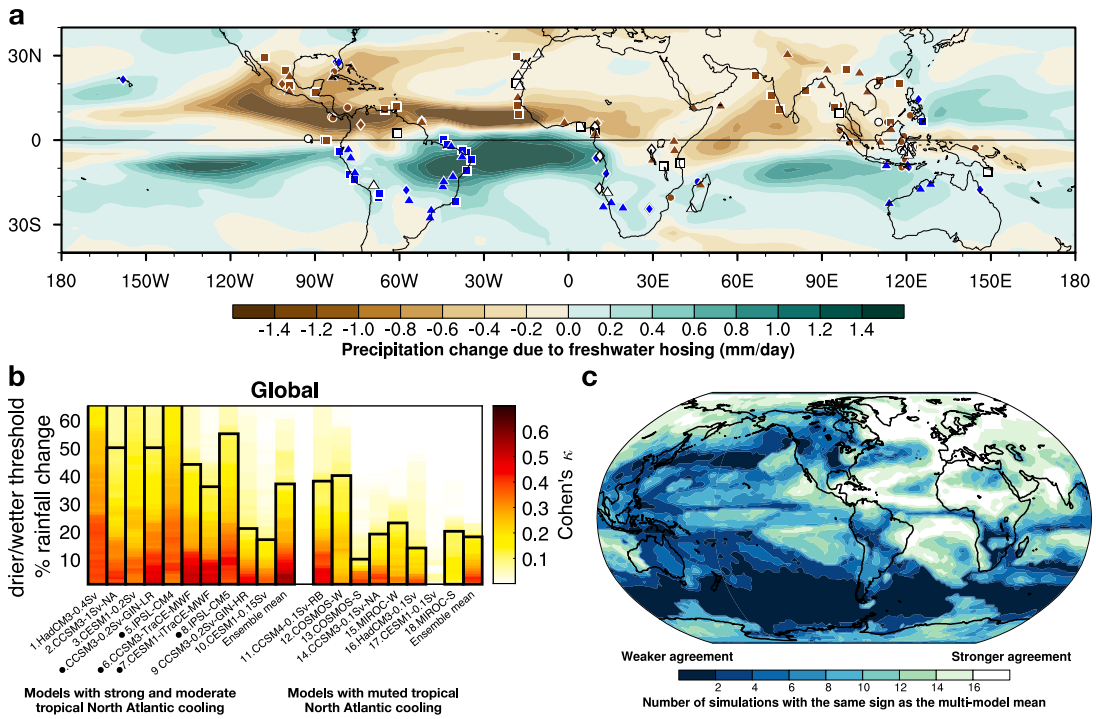

Fig. 1. Tropical rainfall changes in response to a weakened AMOC. (a) 154 hydroclimate-sensitive paleoclimate proxy records (symbols) indicating wetter (blue), drier (brown), or unchanged (white) conditions during HS1 compared to a LGM/deglacial reference interval (DiNezio et al., 2025a). The shape of the symbol indicates terrestrial isotope (triangle), marine isotope (circle), aridity (square), and vegetation (diamond) proxy records. Colored shading indicate the ensemble mean annual rainfall change (mm/day) for the 5 simulations that have the highest global model-data agreement (CCSM3-TraCE-MWF, CCSM3-0.2Sv-GIN-LR, CESM1-iTraCE-MWF, IPSL-CM5, and IPSL-CM4). (b) Agreement between the simulated and proxy-inferred patterns of rainfall change based on the Cohen's κ statistic (Cohen, 1960). Cohen's κ for each simulation shown as a function of the drier/wetter threshold (0%–60%). Black outlines indicate statistically significant values ($p < 0.05$). The highest κ for each simulation is listed in (Table 1). The simulations are grouped based on the tropical North Atlantic temperature change (12°–22°N, 80°–40°W; Table 1). Simulations with an average temperature change less than −1 °C are classified as the "strong and moderate cooling" group, while those with changes greater than −1 °C fall into the "muted cooling" group. The ensemble mean for each grouping is also provided. Black dots next to the model names indicate the simulations used in (a). (c) The number of simulations with the same sign as the 18-member ensemble mean rainfall response (Fig. 2, bottom row). Globally, the proxy-inferred patterns of hydroclimate change during HS1 best agree with the simulations with strong and moderate cooling of the tropical North Atlantic.

exhibit large departures at the regional level. For example, over land where monsoonal responses may not be directly driven by the global shift in the ITCZ (Biasutti et al., 2018). The extent of the ITCZ shift also varies zonally. The most pronounced southward shifts occur over the Atlantic, eastern Pacific, and Indian Oceans, whereas the changes show a large spread over land and the western and central Pacific (Fig. 4a).

We find that the magnitude of tropical North Atlantic cooling is a key factor controlling the agreement between the simulations and proxy-inferred responses. Although all freshwater hosing simulations show cooling across the high-latitude North Atlantic (Figure S1), the simulations with moderate and strong cooling of the tropical North Atlantic (12°–22°N, 80°–20°W; Fig. 3a) produce rainfall responses (Fig. 3b) that best agree with the proxy-inferred patterns of rainfall changes during HS1 (Figs. 1b and 5a blue line). Simulations with muted cooling of the tropical North Atlantic (Fig. 3c) show poorer agreement with the proxy-inferred patterns (Figs. 1b, 3d, and 5a orange line). The importance of tropical North Atlantic cooling for the model-data agreement is robust across the entire global tropics (Fig. 5a), as well as for regions both within (Fig. 5b) and outside (Fig. 5c) the Atlantic ITCZ domain. This finding is also consistent across all proxy types (Fig. 5).

Notably, the model-data agreement is not directly related to the magnitude of the AMOC reduction (Figure S8a and S8b). For instance, both COSMOS-W and MIROC-S have a large AMOC reduction (17.9 and 16.0 Sv, respectively; Table 1), but only weak agreement with the proxy-inferred patterns. The temperature change in the tropical North Atlantic is also poorly correlated with the reduction in AMOC (Figures S8c and S8d). Furthermore, although the simulations exhibit the well-known double ITCZ precipitation bias in the Southern Hemisphere (Tian and Dong, 2020) (Figure S9a), this systematic model issue does not significantly affect the agreement between the simulated and proxy-inferred rainfall pattern (Figure S9b). Collectively, these results further reinforce the robust link between tropical North Atlantic cooling and the overall model-data agreement. The following results sections further explore the regional rainfall responses and associated mechanisms, here organized by ocean basin.

3.1. Rainfall changes across the tropical Atlantic Ocean

The proxy-inferred and simulated rainfall changes in response to a weaker AMOC are generally the most consistent in Atlantic regions (Figs. 1a and 5b). A southward shift of the Atlantic ITCZ provides a first-order explanation for the observed patterns (Fig. 4). However, some regional rainfall responses show departures from the patterns of rainfall change expected from a simple meridional ITCZ shift. For example, in West Africa, a drying during HS1 extends into the Sahel, but is limited to more coastal proxy records west of 10°E. Proxy records from sites along the eastern Gulf of Guinea, the Congo, and further south along the west coast of Africa do not show clear evidence of a Heinrich event, suggesting a muted response in these locations. The absence of a clear HS1 signal in proxy data from coastal southwestern Africa is in stark contrast with sites at similar latitudes in South America, where many proxy records indicate wetter conditions during HS1 (Fig. 1a). Such patterns require more nuanced mechanisms as discussed in Sections 3.1.1 and 3.1.2.

3.1.1. Drier northern South America and wetter northeastern Brazil

Our proxy synthesis shows widespread drying across northern South America (0–12°N, 60°–80°W) during HS1 (Fig. 1a). South of this

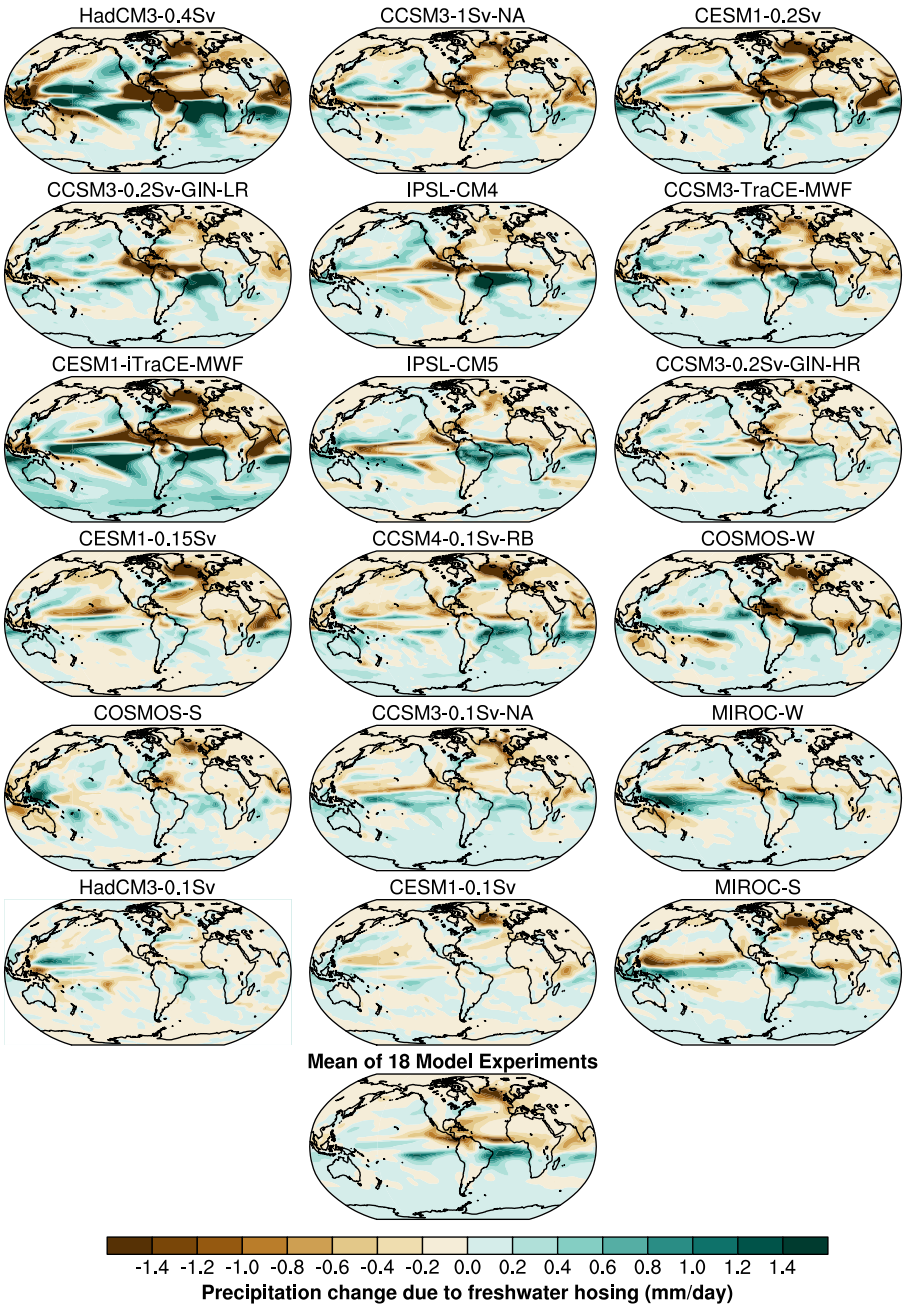

Fig. 2. Simulated annual mean precipitation change in response to freshwater hosing (mm/day) for the 18 freshwater hosing simulations (Table 1). The ensemble mean including all 18 simulations (bottom row).

region, the proxy records reveal wetter conditions, particularly over northeastern Brazil (0–20°S, 35°–55°W). This spatial pattern agrees well with the ensemble mean of freshwater hosing simulations (Fig. 2), which show reduced precipitation over northern South America and increased precipitation over northeastern Brazil and the central Andes. The strong model-data agreement allows us to use the simulations to diagnose the mechanisms driving the proxy-inferred changes.

The decrease in precipitation north of the equator and increase in precipitation south of the equator suggests a southward shift of the ITCZ in the Atlantic and eastern Pacific (Deplazes et al., 2013). According to well-established theoretical and modeling studies, these rainfall changes occur through a reorganization of the ascending branch of the Hadley Circulation in order to compensate for the inter-hemispheric energy imbalance caused by the AMOC weakening (Zhang and Delworth, 2005; Clement and Peterson, 2008; Marshall et al., 2013; Swingedouw et al., 2009; Schneider et al., 2014). The strongest precipitation changes occur over the ocean, with the impact of the ITCZ shift extending inland into South America (Fig. 2). We find that almost all the simulations show a southward shift of the ITCZ across the Atlantic and the eastern Pacific Ocean, suggesting that a southward shift of the ITCZ over this region is a robust response to freshwater forcing (Fig. 4a). The latitudinal extent of the Atlantic ITCZ shift is strongly correlated with changes in tropical North Atlantic temperature (Fig. 4b).

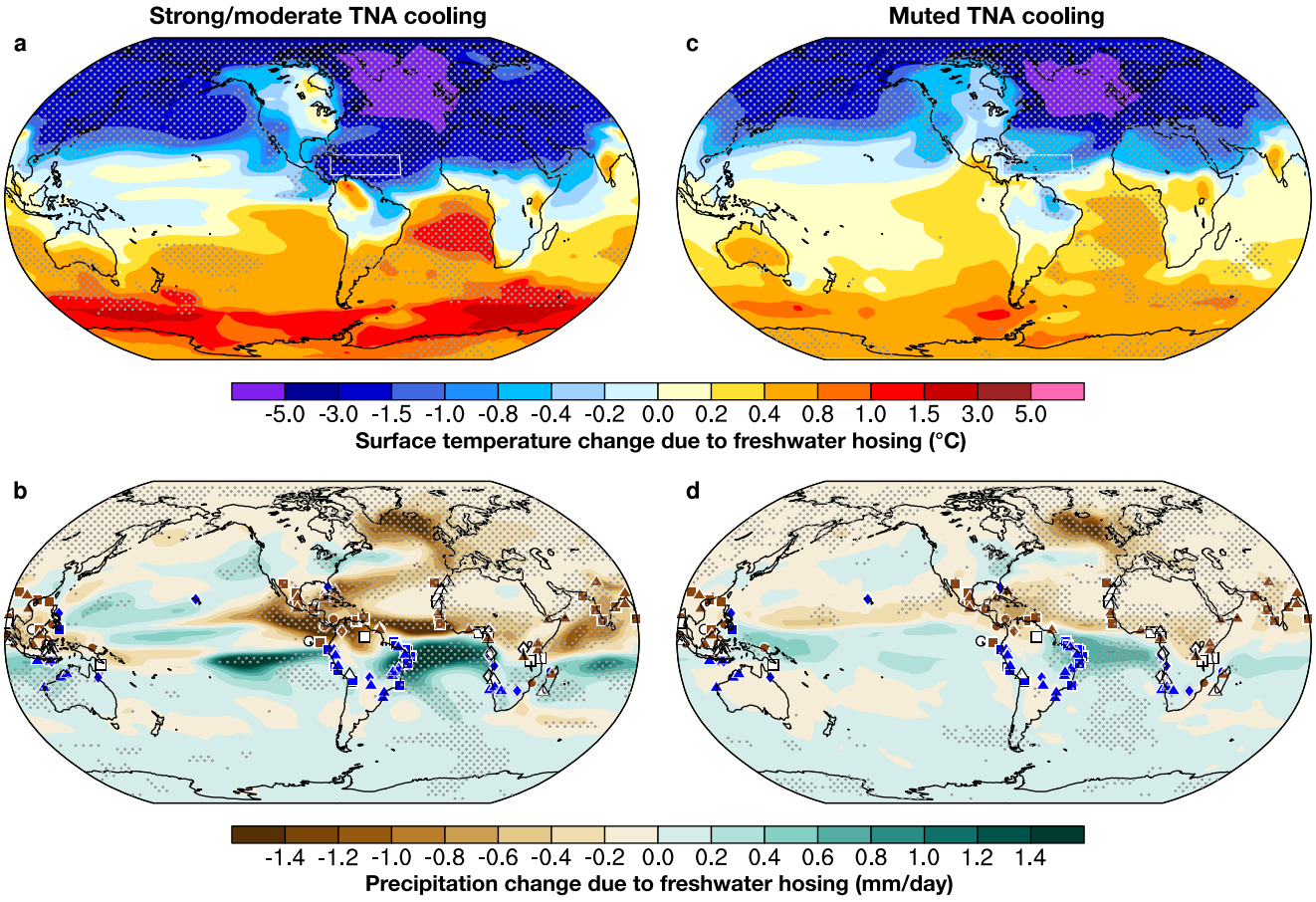

Fig. 3. Ensemble mean temperature and precipitation changes in the freshwater hosing simulations with (a, b) strong and moderate and (c, d) muted cooling of the tropical North Atlantic (TNA: 12°–22°N, 80°–40°W, white box). Model groupings are provided in Table 1 and Fig. 1b. Changes in (a, c) surface air temperature (°C) and (b, d) precipitation (mm/day). Stippling indicates where all or all but one member agree on the sign of the respective ensemble mean precipitation or temperature change. The rainfall changes inferred from the proxy records are indicated by the symbols in (b, d) as in Fig. 1a.

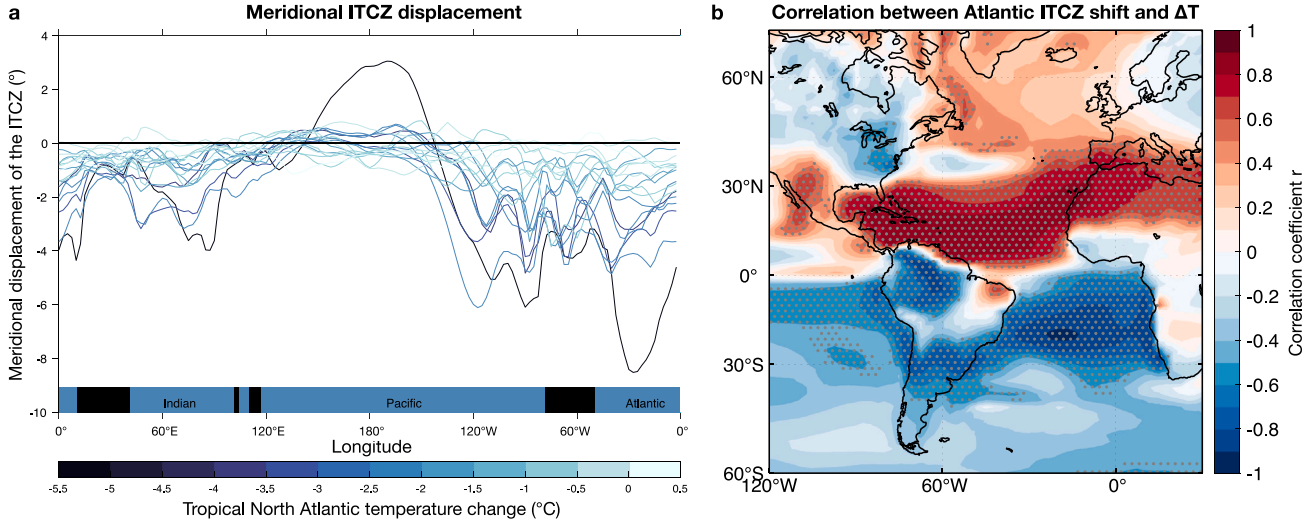

Fig. 4. Atlantic ITCZ position controlled by tropical North Atlantic temperature. (a) Meridional displacement of the ITCZ due to freshwater hosing over the global tropics. The ITCZ meridional displacement is based on the changes in the latitude of the centroid of the tropical rain belt (McGee et al., 2018). A positive (negative) value on the y-axis indicates a northward (southward) shift of the ITCZ. Color scale indicates the tropical North Atlantic temperature change in each simulation. The horizontal blue bars at the bottom indicate ocean basins, and the black bars indicate the continents. (b) Spatial correlation between the magnitude of the Atlantic ITCZ shift and changes in surface temperature across the 18 simulations. Stippling indicates significant correlations ($p < 0.05$).

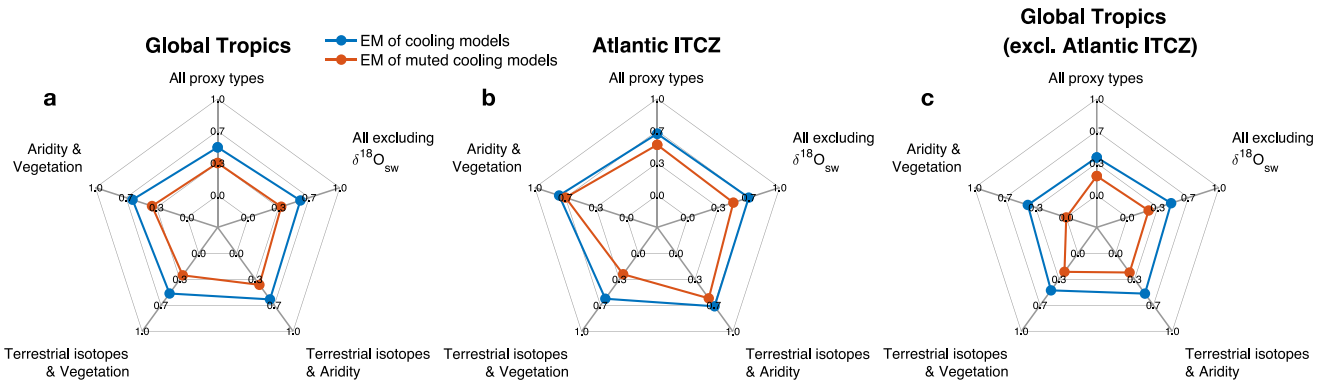

Fig. 5. Sensitivity of model-data agreement based on regional domain and proxy category. Cohen's κ for the ensemble mean of simulations with strong and moderate (blue) and muted (orange) cooling of the tropical North Atlantic (Fig. 3a, c) for (a) the entire global tropics, (b) the Atlantic ITCZ domain, and (c) the global tropics excluding the Atlantic ITCZ. The Cohen's κ is provided for all proxy types, as well as various subsets of the different proxy categories (e.g., aridity and vegetation proxies only, or all proxies except for $\delta^{18}O_{sw}$ (Section 2.1).

Precipitation across northern and eastern tropical South America are correlated with tropical Atlantic temperature changes (Fig. 6). While the rainfall changes in northern South America are strongly correlated with tropical Atlantic SST (Fig. 6a, b), the rainfall changes in northeastern Brazil are better correlated with tropical south Atlantic SST (Fig. 6c, d). Together, these correlation patterns suggest AMOC-induced changes in the tropical Atlantic SST gradient are important for precipitation across tropical South America.

The northeast trade winds intensify in response to the AMOC-induced changes in the inter-hemispheric meridional SST gradient (Figure S4, annual mean). The strengthened winds increase evaporative cooling which further contributes to tropical North Atlantic cooling via the wind-evaporation-SST (WES) feedback (Xie and Philander, 1994). The WES feedback also contributes to warmer temperatures across the tropical South Atlantic due to the weaker southeast trade winds (Figure S4, annual).

AMOC-induced changes in the tropical Atlantic SST gradient and the location of the ascending branch of the Hadley circulation are key controls on precipitation across tropical South America. The reduction in AMOC strength may also weaken or reverse the North Brazil Current and further contribute to cooling in the tropical North Atlantic and warming in the tropical South Atlantic by impacting the northward heat transport in this region (Wen et al., 2011). Previous work by Campos et al. (2019) find that millennial-scale precipitation in South America is sensitive to both dynamic and thermodynamic processes, including seasonal moisture supply from the tropical Atlantic. A cooler tropical North Atlantic decreases the water vapor content in the air that is advected from the tropical North Atlantic to northern South America via the climatological northeast trade winds (Figure S5), which further contributes to reduced rainfall (Figure S4). Similarly, warming of the tropical South Atlantic increases the moisture content of the air transported by the southeast trade winds to northeastern Brazil (Figure S4).

3.1.2. *Aridification of West Africa*

The freshwater hosing simulations and proxy data provide evidence for widespread drying across the western Sahel in northwestern tropical Africa (5°–15°N, 18°W–10°E) (Fig. 1), an area influenced by the west African monsoon. Similarly to South America, this change has previously been attributed to the southward shift of the Atlantic ITCZ during HS1 (Stager et al., 2011). Analysis of the freshwater hosing simulations suggests a more complex response in which drying over the Sahara and Sahel is controlled by several indirect responses to the cooling of the North Atlantic. In all simulations, cooling of the North Atlantic causes widespread and seasonally persistent surface cooling over Africa north of 15° N (Figures S1 and S4). This surface cooling weakens the Saharan Heat Low, decreases the meridional sea level pressure gradient between the Sahara and the Guinea coast, and reduces the northward propagation of low-level moist southwesterly winds during the boreal summer monsoon season (June–July–August, JJA; Fig. 7a) consistent with the mechanisms proposed by Liu et al. (2014). In addition, there is a weakening of the upper tropospheric Tropical Easterly Jet (TEJ) in the simulations (Fig. 7c), which may further weaken the West African Monsoon by reducing upper-level divergence and low-level convergence (Sylla et al., 2009; Nicholson, 2008).

The simulations show the largest rainfall reductions near the Atlantic coast and a west to east decline in the magnitude of the drying (Figs. 1a and 3b, d) that mimic the climatological rainfall gradient (Figure S3). In this region, changes in the mid-tropospheric African Easterly Jet (AEJ; Fig. 7b) contribute to the drying in West Africa through intensified moisture export (Mulitza et al., 2008) and its impact on convection core genesis (Cook, 1999; Diongue et al., 2002; Mohr and Thorncroft, 2006; Fontaine et al., 2010). In the simulations with seasonal output available (Figure S4), a weakened mid-tropospheric meridional temperature gradient between the tropical North Atlantic and the Gulf of Guinea weakens the AEJ over the coastal northwestern tropical Africa region (Fig. 7b), and as a result, causes further drying across this region during the summer monsoon season (Fig. 7a).

The role of tropical Atlantic temperature is further supported by a strong correlation between tropical North Atlantic temperature and precipitation across coastal northwestern tropical Africa ($r \approx 0.7$, Fig. 7d). The influence of tropical Atlantic temperature weakens inland, as evidenced through a gradual weakening of the correlation between tropical North Atlantic temperature and northern tropical Africa precipitation moving eastward (Fig. 7d). A strengthening correlation with high-latitude North Atlantic temperature (40°–65°N, 60°W–0°) suggests a stronger influence of high latitude temperature on northern tropical Africa precipitation east of the prime meridian (Fig. 7d) as further discussed in Section 3.2.1.

3.2. *Monsoonal responses across the Indian Ocean*

Proxy records from around the Indian Ocean, which includes the Indian subcontinent, eastern equatorial and southeastern Africa and western Australia (Fig. 1a), indicate substantially less conclusive evidence for widespread drought during HS1 compared with previous syntheses (Stager et al., 2011). Our synthesis does not clearly show the extension of HS1 aridity into equatorial or southeastern East Africa. Instead, drier conditions are restricted to the Indian subcontinent and northeastern Africa (10°–20°N, 30°–50°E), and wetter conditions are

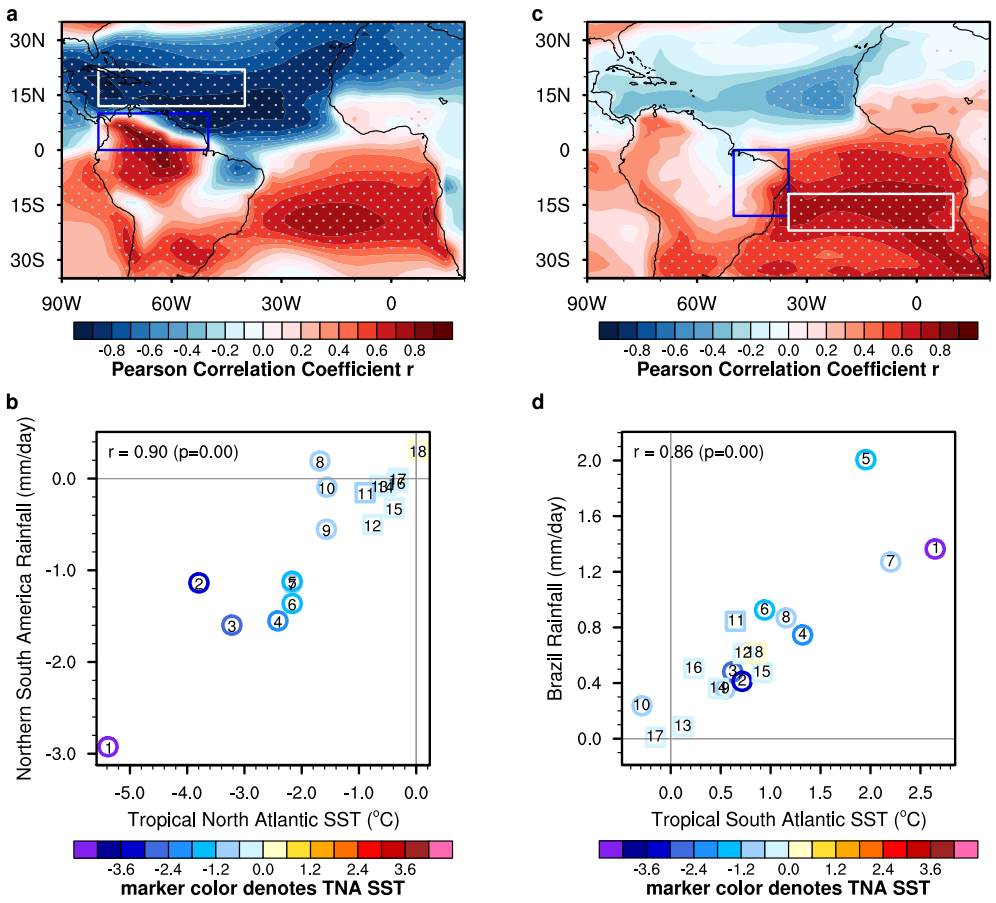

Fig. 6. Tropical Atlantic temperature controls precipitation changes over northern and eastern South America. (a) Spatial correlation between simulated rainfall changes over northern South America (blue box) and surface temperature changes. (b) Scatter plot of rainfall changes over northern South America (blue box in panel a) versus surface temperature changes over the tropical North Atlantic (white box in panel a). (c) Spatial correlation between rainfall changes over eastern South America (blue box) and surface temperature changes. (d) Scatter plot of rainfall changes over eastern South America (blue box in panel c) versus surface temperature changes over the southern tropical Atlantic (white box in panel c). Stippling in (a) and (c) indicates significant correlations (two-tailed t-test at the 90% confidence level, Section 2.2). Markers in panels b and d are numbered based on Table 1 and colored to denote the tropical north Atlantic temperature change (°C). Circles indicate the simulations with strong and moderate tropical North Atlantic cooling. Squares indicate the simulations with muted cooling.

only evident in southeastern Africa (15°–20°S, 25°–35°E) and northern Australia (10°–25°S, 110–150°E) (Figs. 1 and S1). We find that rainfall over equatorial east Africa remained largely unchanged during HS1. A number of lake records, for example Lake Tana (Lamb et al., 2007) and Lake Victoria, previously interpreted as desiccated by Stager et al. (2011) are excluded from our synthesis due to the lack of an LGM or deglacial baseline prior to HS1 that prevents us from evaluating whether there was a distinct change during HS1 or if the deglacial lake level rise simply reflects a wetter transition from a dry LGM state (Section 2.1).

Precipitation changes over the Indian Ocean show complex spatial features, seasonality, and model dependence. The pattern of drier conditions over the northern tropical Indian Ocean and wetter conditions over the southern tropical Indian Ocean that are separated by a transition zone with small changes, is a robust feature of freshwater hosing (Figs. 1a and 2). Some insights into the causes of these changes are provided by a subset of the simulations for which we have seasonal output (Section 2.2). In these simulations, the annual mean response is dominated by changes in summer monsoon precipitation over most of the Indian Ocean domain. The drying over India is most pronounced during boreal summer (Fig. 8a; JJA), whereas in southeast Africa and northern Australia, wetter conditions are strongest during austral summer (Fig. 8b; DJF).

While many of the simulations show basin-wide drying over the northern tropical Indian Ocean, five of the freshwater hosing simulations show zonally asymmetric precipitation changes between 12°N and 12°S (Fig. 2; CESM1-0.2Sv, CESM1-0.15Sv, CESM1-0.1Sv, CESM1-iTraCE-MWF, and CCSM3-0.1Sv-NA). The pattern of drier conditions in the western Indian Ocean and East Africa and wetter conditions in the eastern Indian Ocean is consistent with a zonal mode during HS1 identified by Du et al. (2023) using CESM1-iTraCE. However, this pattern is model-dependent and the majority of the simulations from other models do not exhibit this asymmetry as further discussed in Section 3.3.2 about the Maritime Continent.

3.2.1. *Drying across northeastern equatorial Africa*

The proxy data and freshwater hosing simulations consistently show drier conditions over northeastern equatorial Africa (Figs. 1a and 2). While the rainfall changes in northwestern equatorial Africa are strongly correlated with tropical Atlantic SSTs (Section 3.1.2), this correlation decreases longitudinally from west to east across Africa (Fig. 7d). Rainfall changes in northeastern equatorial Africa are poorly correlated with tropical Atlantic SST changes, and are instead better correlated with high latitude temperatures (Fig. 7d).

The drier conditions across northeastern Africa in response the AMOC reduction are explained by the advection cold, dry air from higher-latitudes into northeastern Africa (Figure S4) (Chou et al., 2001). The ventilation mechanism is consistent with year-round drying in the freshwater hosing simulations (Figure S4, annual) as stabilization of the atmosphere with cooler high latitude air inhibits deep convection during the rainy seasons.

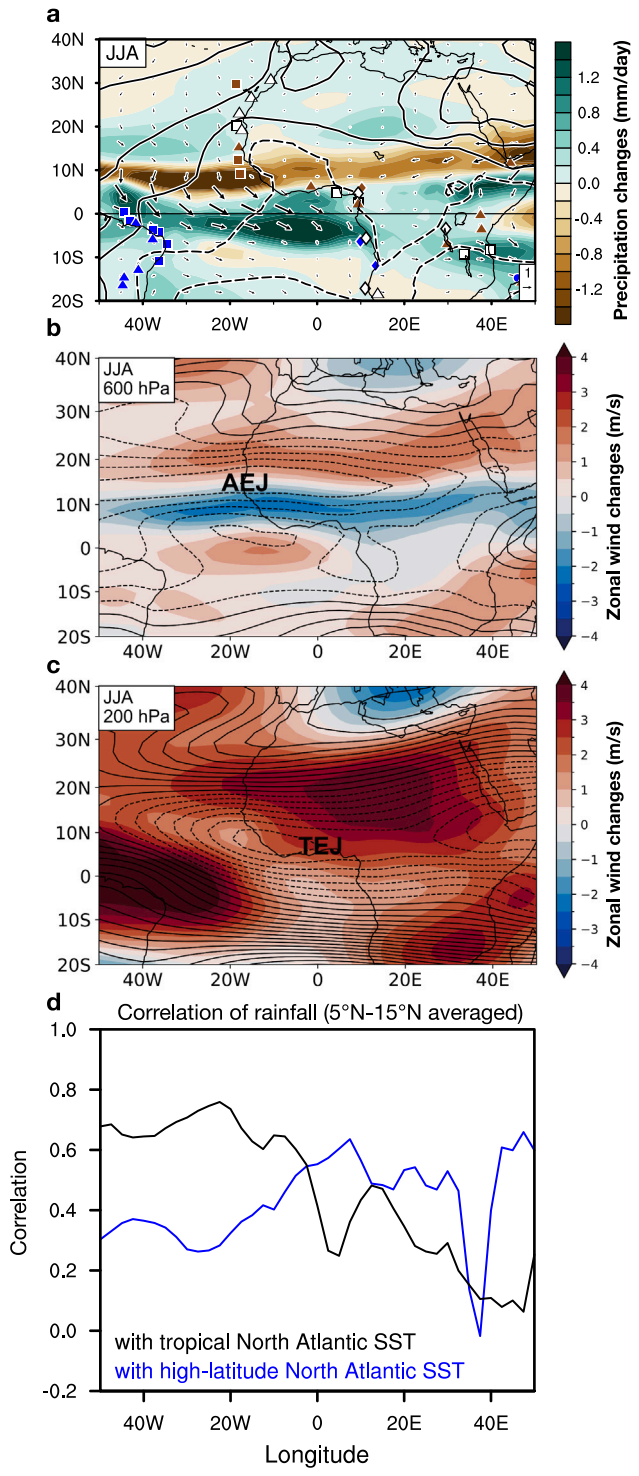

Fig. 7. Large-scale atmospheric response to tropical North Atlantic cooling weakens the Western African Monsoon. (a) Changes in precipitation (shading), surface winds (arrows), and sea-level pressure (contours) in June–July–August (JJA). Solid contours indicate positive SLP changes and dashed contours indicate negative SLP changes. Proxy records as in Fig. 1a (symbols). (b) Changes in 600 hPa zonal wind (shading) and climatological 600 hPa zonal wind (contours; solid: positive values, dashed: negative values). Positive zonal wind changes (red shading) indicate anomalous westerly flow (i.e., weakened easterly winds). The position of the African Easterly Jet (AEJ) is denoted. (c) Changes in 200 hPa zonal wind (shading) and climatological 200 hPa zonal wind (contours). The position of the Tropical Easterly Jet (TEJ) is denoted. Panels a–c show the ensemble mean of the four models with monthly climate output available (IPSL-CM5, CESM1-0.2Sv, CCSM3-1Sv-NA, and CESM1-iTraCE-MWF, Figures S10-S13). (d) Correlation coefficients of rainfall changes in North Africa (5°N–15°N) with temperature changes in the tropical North Atlantic (black: 12°–22°N, 80°–40°W) and high-latitude North Atlantic (blue: 40°–65°N, 60°W–0°) as a function of longitude.

3.2.2. Aridification of the Indian subcontinent

Drying across the Indian subcontinent is a robust response of the climate system to a weaker AMOC. All of the freshwater hosing simulations except CCMS3-0.1Sv-NA produce drying over the Indian subcontinent (Figs. 1c and 2). Previous work by Marzin et al. (2013) suggested that tropical Atlantic SST changes are key to explain the reduction of rainfall over India, inducing a southward shift of the subtropical westerly jet across northern Africa and Eurasia and reducing the meridional upper tropospheric temperature gradient between the Tibetan Plateau and the tropical Indian Ocean. Together these changes decrease the intensity of the summer monsoon. However, drying over India is also present in simulations with weak cooling of the tropical North Atlantic (Fig. 3c, d), suggesting that other mechanisms are involved to generate more arid conditions.

Work by Mohtadi et al. (2014) find that the Indian summer monsoon responds to North Atlantic cooling through a stationary Rossby wave train teleconnection that originates in the North Atlantic. An alternative mechanism is that cooling of the Arabian Sea via the advection of cold, mid-latitude air acts as an important bridge between high-latitude cooling and India summer monsoon rainfall, and provides a possible dynamical explanation for the simulated decrease of Indian summer monsoon rainfall in previous studies (e.g. Pausata et al., 2011). As discussed in Section 3 results overview, the high-latitude North Atlantic cools in response to freshwater forcing. The Northern Hemisphere westerlies advect cold and dry air downstream to lower latitudes, but due to the topographic insulating effect of the Himalayas, this high latitude cooling cannot directly influence the Indian subcontinent through the process of ventilation (Boos and Kuang, 2010). Instead, the cold air is advected across the Arabian Peninsula into the northwestern Arabian Sea (Fig. 8) where it is not blocked by high topography. The intrusion of this cold, dry air over the Arabian Sea reduces moisture availability during the summer monsoon. This effect produces widespread drying over the Indian subcontinent even in simulations where Indian summer monsoon winds do not weaken, demonstrating the thermodynamic nature of the response.

The relative importance of high latitude versus tropical North Atlantic cooling in controlling changes in Indian summer monsoon rainfall appears to be model dependent. For example, simulations with similar amounts of high latitude cooling but varying magnitudes of tropical North Atlantic cooling (Fig. 3a, c) show a relationship between the magnitude of the rainfall reduction over India and tropical Atlantic temperatures (Figs. 3b, d and 8e). Thus, it appears that both high and low-latitude mechanisms influence precipitation in India, but the relative importance in each simulation likely depends on the relative magnitudes of surface temperature changes in the tropical and high-latitude North Atlantic.

An alternative hypothesis to explain the drying of the Indian subcontinent is that precipitation across India weakens as a result of a Rossby wave response to suppressed convective heating over Indonesia in the Maritime Continent (Zhang and Delworth, 2005). However, the simulations do not consistently agree on the sign of the precipitation change in the Maritime Continent, with approximately half of the simulations showing wetter and half showing drier conditions (Section 3.3.2). The rainfall discrepancies over the Maritime Continent make it difficult to evaluate this mechanism, but given that drying over India is a consistent response in nearly all simulations, this mechanism appears to be of secondary importance.

3.2.3. Wetter southeastern Africa and northern Australia

The freshwater hosing simulations generally show wetter conditions across the tropical to subtropical southern Indian Ocean from Africa to Australia. The increase in rainfall is most pronounced during the austral summer wet season (Figs. 8b and 8d, DJF), when the region receives more moisture via the climatological winds (Figure S5). Strong cooling in the Arabian Sea increases the north–south temperature and sea level pressure (SLP) gradient, driving northerly wind anomalies

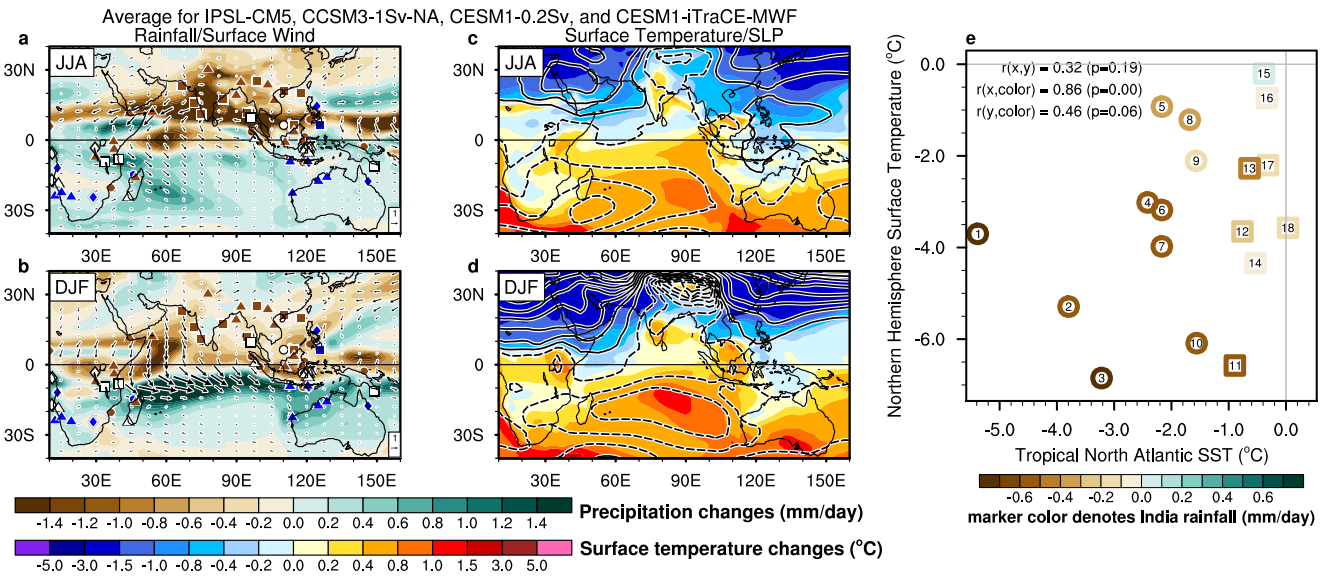

Fig. 8. Simulated temperature and precipitation changes for the Indian Ocean domain. Rainfall (shading, mm/day) and surface wind (arrows, m/s) changes for (a) June–July–August (JJA) and (b) December–January–February (DJF) due to freshwater hosing. Overlain are the proxy records and their interpretations (Fig. 1a). Seasonal surface temperature (shading, °C) and SLP (contours, 0.5 hPa interval) changes for (c) JJA and (d) DJF. Dashed contours indicate negative SLP changes. Solid contours indicate positive SLP changes. (e) Scatter plot of Northern Hemisphere versus tropical North Atlantic temperature changes for the 18 freshwater hosing simulations (Table 1). Marker color denotes the rainfall changes in India (mm/day). Symbols indicate the strong and moderate (circles) and muted (squares) tropical North Atlantic cooling groups.

across the equator (Fig. 8b and d). The northerly wind anomalies are deflected by the Coriolis effect in the Southern Hemisphere to become northwesterly wind anomalies that subsequently weaken the climatological southeast trade winds, reduce evaporative cooling and induce SST warming via the WES feedback along 15°S (Figs. 8b and 8d). Through such a WES feedback (Sections Section 3.1.1), there is a broad band of positive rainfall anomalies at ~15°S (Fig. 8b) during DJF, indicating a southward shift of the rain belt over the tropical Indian Ocean (Fig. 4a). These changes provide additional moisture, which is then transported to southeastern Africa via the climatological easterlies (Figure S5), yielding wetter conditions in southeastern Africa even without a large change in wind.

The wetter conditions in northern Australia are not only affected by the shift in the tropical rain belt, but also by coastal warming along the western coast of Australia (Fig. 8d). The coastal SST warming could be related to a strengthened southward Leeuwin Current. Northerly wind anomalies along the west coast of Australia advect warm tropical waters into this region. This mechanism is supported by the similarity between the simulated pattern of warming along the west coast of Australia (Figure S4) and the position of the climatological Leeuwin Current. Although the causality of the coastal warming and northerly wind anomalies requires further investigation, the combined impact of warm SST and northerly wind anomalies intensify the wetter conditions over northwestern Australia through enhanced moisture availability and strengthened summer monsoon winds. In summary, cooling of the Arabian Sea and the associated northerly wind anomalies are important for communicating the high-latitude North Atlantic cooling to the southern tropical Indian Ocean.

3.3. Rainfall changes across the tropical Pacific Ocean

Conversely, the rainfall changes across the Maritime Continent are heterogeneous. In many records from Indonesia, the rainfall changes during HS1 are muted and difficult to unambiguously classify as wet or dry due to large background noise. A few notable exceptions are a stalagmite record from Borneo (Partin et al., 2007) and three marine salinity records from Sumatra on the western margin of the Maritime Continent in the Indian Ocean (Mohtadi et al., 2014). Collectively, the proxy records generally indicate that conditions were unchanged or drier across the Maritime Continent during HS1. The regional responses are further described in Sections 3.3.1 and 3.3.2.

3.3.1. Wetter tropical Andes

The proxy synthesis shows that the Andes mountains south of the equator, herein the Peruvian Andes (0–15°S), are wetter during HS1 compared to the LGM. This is consistent with the freshwater hosing simulations, which show increased precipitation across this region (Fig. 1a). Wetter Peruvian Andes are shown in simulations with and without tropical North Atlantic cooling (Fig. 3), suggesting that tropical North Atlantic SST is not a deterministic factor for precipitation change over the Peruvian Andes.

Located just south of the equator, the Peruvian Andes are sensitive to a meridional ITCZ shift. Nearly all models simulate a southward shift of the ITCZ in the eastern Pacific Ocean, though the models with weak tropical North Atlantic cooling generally show a smaller change in the latitude of the eastern Pacific ITCZ (Fig. 4a). A southward displaced eastern Pacific ITCZ, driven by the interhemispheric temperature imbalance, thus accounts for the increased Andes precipitation.

Further south, over the Central Andes and the Altiplano (15–25°S) - which consists of the highlands of southern Peru, western Bolivia, and northern Chile — four records (Thompson, 1998; Ramirez et al., 2003; Fornace et al., 2014; Nunnery et al., 2018) show no change, while two records (Baker et al., 2001; Placzek et al., 2006) show wetter conditions during HS1 (Fig. 1a). Collectively, these records suggest that the Altiplano was slightly wetter during HS1. However, not all proxies may capture this nuanced change. In particular, the two records that show wetter conditions are both aridity records (Fig. 1a; square symbols).

Consistent with the proxy data, a wetter Altiplano is shown in the model ensemble with tropical North Atlantic cooling (Fig. 3a, b). The magnitude of tropical North Atlantic cooling thus plays a critical role in modulating the precipitation change over the Altiplano. This relationship is evidenced by the strong negative correlation between the precipitation change over the Altiplano and tropical North Atlantic temperature (Fig. 9a), with the negative correlation extending into the tropical northeastern Pacific. We find that in the simulations with tropical North Atlantic cooling, anomalously high sea level pressure strengthens the northeasterly trade winds across the Central America isthmus. The strengthened trade winds propagate the drying and cooling signals from the tropical North Atlantic to the northeastern tropical Pacific (Figure S4, annual), in agreement with an Atlantic-Pacific atmospheric bridge mechanism (Zhang and Delworth, 2005; Timmermann

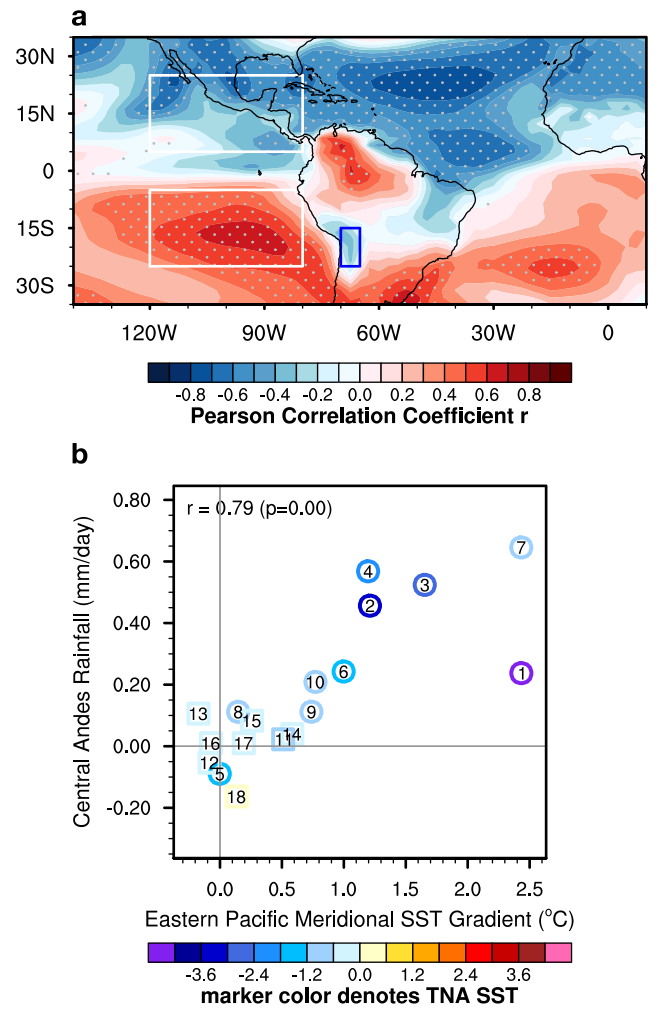

Fig. 9. Controls on rainfall changes over the central Andes. (a) Spatial correlation between rainfall changes over the Central Andes (outlined by the blue box) and surface temperature changes. Stippling indicates a significant correlation (Section 2.2). (b) Scatter plot of rainfall changes over the central Andes versus changes in eastern tropical Pacific meridional surface temperature gradient (white boxes in a). Symbols denote the simulations with strong and moderate (circles) and muted (squares) tropical North Atlantic cooling.

et al., 2007; Xie et al., 2008; Merkel et al., 2010). Such cross-isthmus dynamics are absent in the simulations with weak tropical North Atlantic cooling (Fig. 3c), where the northeastern tropical Pacific SSTs are warmer instead. A study compiling regional SST records indicates that the transition between cooler tropical northeastern Pacific and warmer tropical southwestern Pacific is located at approximately 2°S (Kienast et al., 2013), supporting the SST patterns simulated in the models with tropical North Atlantic cooling (Fig. 3a).

The change in precipitation over the Altiplano is strongly correlated with the topical eastern Pacific meridional SST gradient (r = 0.79; Fig. 9b). This suggests that the precipitation change is dynamically influenced by changes in large-scale circulation as a response to the spatial pattern of SST change rather than the thermodynamic impact of warming over the adjacent ocean. The tropical northeastern Pacific cooling induces an anomalous meridional sea level pressure gradient with cross-equatorial northerly wind anomalies (Figure S4). Through the WES feedback, stronger northern trade winds enhance tropical Pacific cooling north of the equator, and weaker southern trade winds enhance warming south of the equator, driving a change in the meridional SST gradient over the tropical eastern Pacific. This meridional SST gradient is further enhanced by a Bjerknes feedback (Bjerknes, 1969) that reduces coastal upwelling in the tropical southeastern Pacific and increases SST in the eastern Pacific cold tongue.

Today, the Altiplano is one of the driest climates on Earth's due to its altitude and subtropical location. It is unlikely that the ITCZ shifts to 20°S during HS1 since there is no evidence of such dramatic changes in the proxy data (Fig. 1a). However, we hypothesize based on the seasonality of modern rainfall in the Altiplano (Garreaud et al., 2003), that with a large change in the meridional temperature gradient, the ITCZ would be positioned south enough to occasionally bring tropical convective systems to the Altiplano and cause a slight increase in annual mean precipitation. This may also explain the more nuanced change shown in the proxy data (Fig. 1a).

Lastly, although the ensemble mean of the simulations with tropical North Atlantic cooling shows strong agreement with proxy data over the central Andes, there is poorer inter-model agreement on the spatial pattern of precipitation change, as shown by the absence of stippling in this region in Fig. 3b. The climate of the Andes is difficult to simulate due to the complex topography that may not be adequately represented in global climate models (Neukom et al., 2015). Future studies using high-resolution models with improved representation of the topography and convection-permitting capability will be helpful for better illustrating the climate dynamics of this region. Furthermore, this region is also known to be influenced by changes in the El Niño Southern Oscillation (ENSO) and the Pacific Walker Circulation, where the equatorial and central Andes are wetter during La Niña years and drier during El Niño years (Vuille and Bradley, 2000; Garreaud, 2009; Deser et al., 2012). However, the simulations differ in their responses in the Pacific Walker Circulation, with some models show a more El Niño-like mean Pacific climate state and others showing a more La Niña-like mean state as discussed in Section 3.3.2.

3.3.2. *Heterogeneous rainfall changes across the Maritime Continent*

Intriguingly, the rainfall responses over the Maritime Continent are more complicated than in the eastern Pacific. Whereas the proxy synthesis generally shows muted to drier conditions across the Maritime Continent during HS1, the simulated rainfall responses differ widely (Fig. 2). Approximately half of the simulations simulate drier conditions over the Maritime Continent, while the other half simulate wetter conditions. Although the overall model-data agreement is lower outside of the Atlantic (Fig. 5c), the simulations with moderate to strong cooling of the tropical North Atlantic (Fig. 3a, b) better agree with the proxy synthesis compared to the simulations with weak tropical North Atlantic cooling (Fig. 3c, d).

Rainfall across the Maritime Continent is influenced by both the Pacific and Indian Oceans. The relative influence of each basin on the simulated rainfall change is likely model dependent. To more comprehensively understand the diverse rainfall responses in models, we perform an inter-model Empirical Orthogonal Function (EOF) analysis of the rainfall changes over the Maritime continent (Fig. 10). This analysis allows us to identify the leading modes of inter-model spread of local rainfall responses over the Maritime Continent and explore the connections with global rainfall and temperature responses. The leading inter-model EOF mode of Maritime continent rainfall explains 53% of the total inter-model variability and exhibits a meridional dipole pattern of rainfall over the Indian Ocean (Fig. 10a–c). This meridional dipole is most pronounced in HadCM3-0.4Sv-NA as indicated by the high principal component value (Fig. 10c). The second mode explains 23% of the inter-model variability and features a zonal dipole pattern in the Indian Ocean (Fig. 10d–f). This zonal dipole pattern is particularly strong in CESM1-0.2Sv and CESM1-iTraCE-MWF (Fig. 10f).

The proxy synthesis (Fig. 1a) indicates that both sides of the northern tropical Indian Ocean are drier during HS1, providing independent support of the north-south dipole across the Indian Ocean in EOF1 (Fig. 10a, b). Conversely, a subset of the simulations (e.g., CESM1-0.1Sv, CESM1-0.15, CESM1-0.2Sv, and CCSM3-0.1Sv-NA) demonstrate zonally asymmetric rainfall responses across the Indian Ocean (Fig. 2)

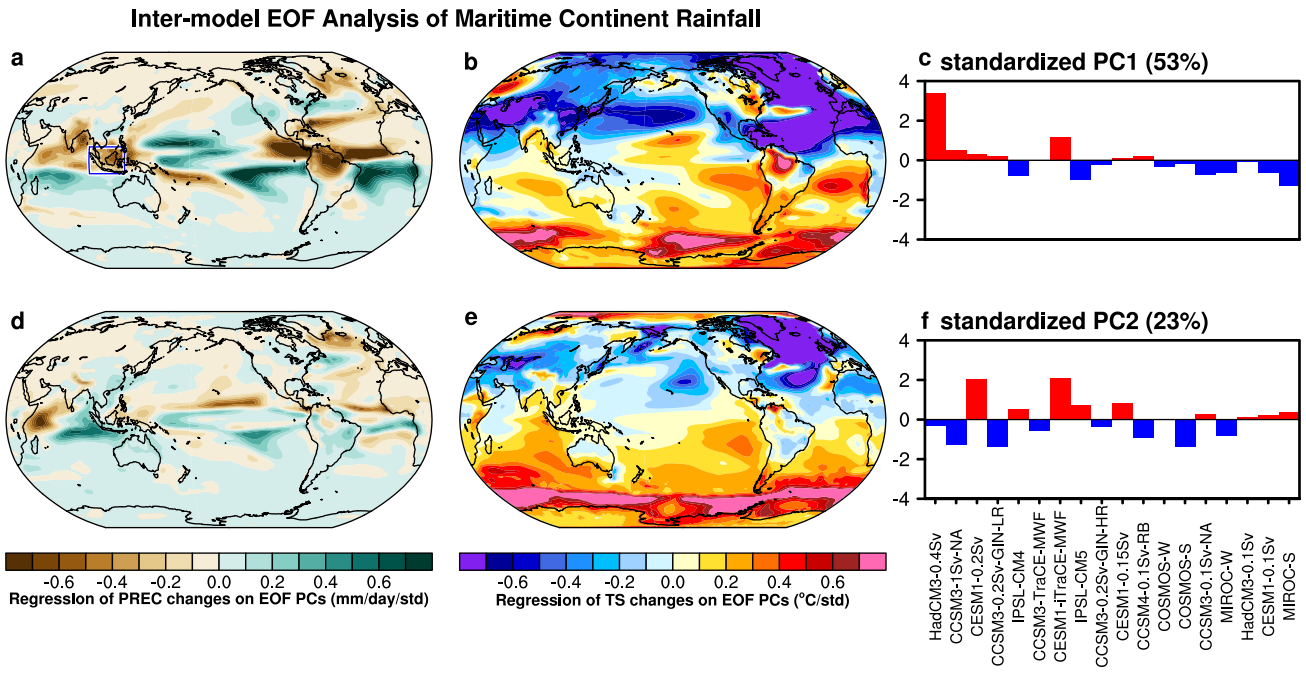

Fig. 10. Inter-model EOF analysis of rainfall changes over the Maritime Continent. The Inter-model EOF analysis is conducted for the precipitation changes over the Maritime continent (outlined by the blue box in a) and the corresponding standardized PC1 and PC2 of inter-model variability are shown in (c) and (f), respectively. Global patterns associated with Maritime continent rainfall changes are obtained by regressing global precipitation (mm/day) and surface air temperature (°C) changes onto the standardized (a, b) PC1 and (d, e) PC2. EOF1 and EOF2 mode explains 53% and 23% of the total inter-model variability, respectively.

that are in line with the EOF2 pattern (Fig. 10d, e), but inconsistent with the proxy-inferred drying observed across the Maritime Continent (Fig. 1).

Global SST regressions on the EOF1 and EOF2 modes show that the rainfall changes over the Maritime Continent are connected to high-latitude North Atlantic cooling and cooling over the Arabian Sea (Fig. 10b, e). However, EOF1 shows stronger connections with SST and rainfall changes in the tropical Pacific and tropical Atlantic, while EOF2 shows a zonal SST dipole pattern over the Indian Ocean and more muted connections to other tropical ocean basins. The simulated wetter conditions over the Maritime Continent in a subset of the simulations may be associated with this east–west SST dipole in the Indian Ocean that may be jointly influenced by high-latitude North Atlantic cooling propagated through the Arabian Sea cooling and/or changes in the Indian Ocean Dipole as suggested by Du et al. (2023). Conversely, drying over the northern tropical Indian Ocean and wetter conditions over the southern tropical Indian Ocean are consistent with strong cooling over the North Atlantic and a southward shift in the ITCZ.

Given that EOF1 explains 53% of the inter-model variability, we also explore mechanisms involving a Pacific pathway by focusing on changes in the Pacific Walker Circulation (PWC). The drying signal across the Maritime Continent is more pronounced in the simulations with tropical North Atlantic cooling (Figs. 3a, b). These simulations also tend to have zonally asymmetric temperature responses in the Pacific, suggesting a PWC influence. The composite of simulations with cooling of the tropical North Atlantic generally shows a zonal asymmetry in equatorial Pacific SSTs and rainfall, with cooler/drier conditions over the western Pacific and warmer/wetter conditions over the eastern Pacific (Fig. 3a, b). This "El Niño-like" pattern hints toward the role of changes in the PWC on tropical rainfall. Of the simulations with full seasonal output available, CCSM3-1Sv-NA shows strong cooling of the tropical North Atlantic (Figures S4 and S11). In CCSM3-1Sv-NA, the cooling of the tropical North Atlantic spreads to northeastern equatorial Pacific by the trade winds and induces warmer and wetter conditions in the southeastern equatorial Pacific (Section 3.3.1). The resulting southward ITCZ shift in the eastern Pacific promotes convection over the southeastern tropical Pacific and subsequently weakens the ascending branch of the Pacific Walker Circulation over the Indo-Pacific warm pool during boreal fall (Fig. 11a). This weaker Walker Circulation mechanism is supported by the wetter signal over the equatorial Andes and an associated increase in convection in the southeastern tropical Pacific.

In contrast, the "El Niño-like" zonal temperature and rainfall asymmetry across the tropical Pacific is absent in other simulations. These simulations generally show SST warming in the eastern Indian Ocean and wetter conditions across the Maritime Continent. This pattern conflicts with the weaker Pacific Walker Circulation mechanism discussed above and results in poor model-data agreement. Most of the models with a wetter Maritime Continent also have weak tropical North Atlantic cooling; however, IPSL-CM5 is an exception. While IPSL-CM5 is one of the models with strong tropical North Atlantic cooling, it shows a strengthening of the PWC and "La Niña-like" pattern in response to freshwater hosing (Fig. 11b), that is consistent with the work of Orihuela-Pinto et al. (2022) that identifies a PWC strengthening with weakened AMOC. In IPSL-CM5, while there is a warming along the tropical Pacific coast of South America, likely associated with a weaker cold tongue driven by the "bridge" mechanism (Zhang and Delworth, 2005; Timmermann et al., 2007; Xie et al., 2008), the stronger Indo-Pacific Warm Pool warming induced by the Indian Ocean dipole dominates the tropical Pacific zonal temperature gradient and drives an "La Niña-like" response (Figure S1). The PWC response to hosing thus appears model dependent.

Given the large disagreement among the simulations and uncertainties in the proxy synthesis, the rainfall response to a weaker AMOC across the Maritime Continent is one of the main drivers of the model-data agreement. Without the full seasonal output from all 18 simulations it is difficult to disentangle competing mechanisms between the Pacific and Indian Oceans. On the proxy side, there is a lack of high-resolution proxy records from the central Pacific to independently validate the simulated Walker Circulation changes. Furthermore, many of the records that show drier responses come from marine isotope records (Fig. 1a) that may also be influenced by an increase in sea surface salinity due to the advection of more saline water from the subtropics as opposed to local rainfall. Furthermore, in many records

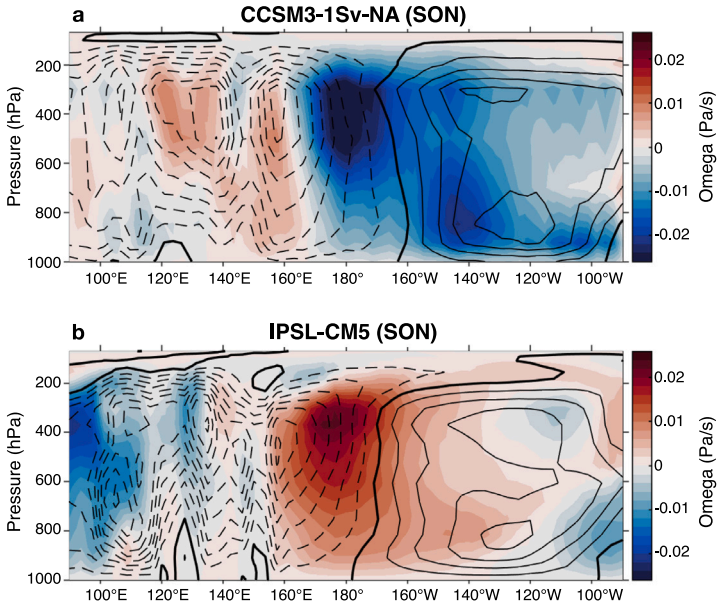

Fig. 11. Simulated Indo-Pacific Walker Circulation changes. Equatorial (5°S–5°N) atmospheric vertical velocity changes (shading; Omega, Pa/s) for September–October–November (SON) for (a) CCSM3-1Sv-NA and (b) IPSL-CM5. Overlain black contours indicate the LGM climatology (0.01 Pa/s contour interval). For the LGM climatology (contours), positive omega values (solid contours) indicate subsidence, and negative omega values (dashed contours) indicate uplift.

it is difficult to clearly identify a wet or dry rainfall signal in many Maritime Continent proxy records due to large background noise.

4. Discussion

4.1. Role of tropical Atlantic SST

Different mechanisms have been proposed to explain how changes in the North Atlantic are transmitted to the global tropics. As reviewed by Clement and Peterson (2008), the mechanisms broadly fall into two categories: zonally symmetric and zonally asymmetric responses. The zonally symmetric mechanisms highlight the role for the cooling over the subpolar North Atlantic to cool the entire mid- and high-latitude Northern Hemisphere via the westerly winds. This cooling is then propagated to the global tropics via strengthened trade winds and the WES feedback, which uniformly shifts the ITCZ southward toward the warmer hemisphere (Broccoli et al., 2006; Chiang and Bitz, 2005; Clement and Peterson, 2008). For the zonally asymmetric mode, Zhang and Delworth (2005) propose that cooling of the tropical North Atlantic increases sea level pressure in the northeastern tropical Pacific, strengthening the cross equatorial trade winds and shifting the eastern Pacific ITCZ southward. The eastern Pacific changes are connected to changes in the western Pacific through a Walker Circulation adjustment, yielding asymmetric rainfall responses across the tropical Pacific (Zhang and Delworth, 2005; Clement and Peterson, 2008).

Although we find evidence of both the zonally symmetric and asymmetric modes in the 18 freshwater hosing simulations, the simulations with an asymmetric response better agree with the proxy data. The proxy records and model ensemble (Figs. 1 and 2) generally show a broad pattern of drier conditions in the Northern Hemisphere and wetter conditions in the Southern Hemisphere that is consistent with the zonally symmetric rainfall response involving a southward shift of the ITCZ. The meridional shift in the ITCZ is particularly pronounced in the Atlantic (Fig. 4a) and is associated with weakening of the AMOC and reduced northward ocean heat transport. Conversely, the proxy-inferred rainfall changes over land and in monsoon regions require more nuanced mechanisms than a zonally symmetric ITCZ shift. Additionally, the differences among the simulations become more pronounced the farther away from the Atlantic, particularly in regions such as the Maritime Continent (Fig. 1c).

We identify that cooling of the tropical North Atlantic is a key driver of global tropical hydroclimate changes. As discussed in Section 3, the simulations with moderate and strong cooling of the tropical North Atlantic (Figs. 1b and 3a, b) better agree with the proxy-inferred patterns compared to simulations with weak tropical North Atlantic cooling (Fig. 3c, d). The ensemble mean of the simulations with tropical Atlantic cooling consistently shows higher global κ compared to the ensemble mean of the simulations with muted cooling across all proxy types (Fig. 5a blue versus orange lines). The importance of tropical Atlantic cooling is further underscored when examining the model-data agreement with and without the Atlantic ITCZ domain (Figs. 5b and 5c).

The subset of simulations with tropical Atlantic cooling tends to show asymmetric rainfall responses in the Pacific with drier conditions across the Maritime Continent and wetter conditions in the eastern equatorial Pacific (Section 3.3.2). Conversely, the subset of simulations with only weak cooling of the tropical North Atlantic (Fig. 3c, d) show a zonally symmetric change in rainfall across the tropical Pacific that is inconsistent with the proxy-inferred responses. This zonal asymmetry is key for producing the correct sign of the rainfall response in regions that are far-removed from the Atlantic.

Furthermore, although a southward shift of the ITCZ in the Atlantic is a robust response in all the simulations (Fig. 4a), the magnitude of tropical North Atlantic cooling strongly influences the hydroclimatic changes in northeastern South America and West Africa. Simulations with stronger cooling of the tropical North Atlantic tend to cause more expansive cooling and drying patterns over the northern South America (Fig. 3a, b). More pronounced southward propagation of drying across South America could limit the spatial extent of wetter conditions emanating from a warmer southern tropical Atlantic. In the eastern side of the basin, stronger tropical North Atlantic cooling shifts the African Easterly Jet and weakens the West African Monsoon along the coast (Section 3.1.2). Together, this highlights that across the Atlantic, there are different mechanisms driving regional responses to freshwater hosing.

4.2. Non-tropical Atlantic SST influences

Although cooling of the tropical North Atlantic emerges as an important explanatory pattern, some regions are impacted by alternative

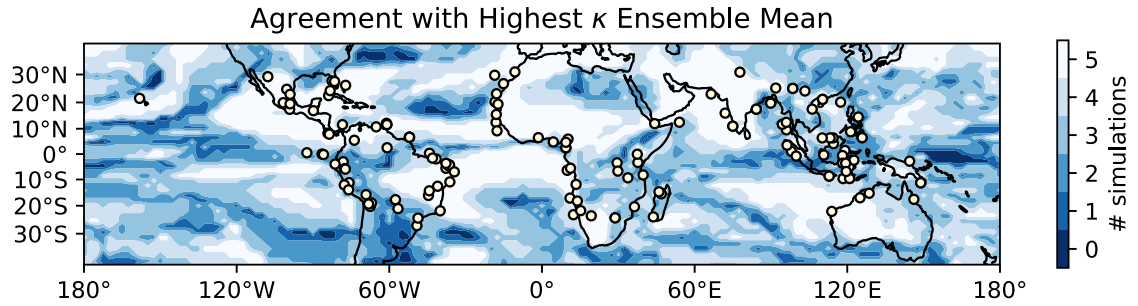

Fig. 12. Simulated multi-model rainfall agreement. The number of hosing simulations that agree on the sign of the ensemble mean rainfall change. Selected simulations are the 5 with the highest model-data agreement based on their global κ (same simulations as Fig. 1a). The sign of the simulated rainfall response (wet/dry/unchanged) is based on a ±5% change in the precipitation rate. Circles indicate the location of the HS1 hydroclimate records (Fig. 1a) to show proxy data coverage.

mechanisms that are not entirely driven by cooling of the tropical North Atlantic. In some regions, temperature changes in the high-latitude North Atlantic or southern tropical Atlantic more directly influence rainfall. For example, advection and high-latitude forcing explain the drying of northeastern Africa (Section 3.2.1). Warming of the southern tropical Atlantic is key for explaining the proxy-inferred rainfall changes in South America (Section 3.1.1).

Furthermore, there are regions that appear linked to both high-latitude and tropical mechanisms. Drier conditions in the Indian monsoon region occur regardless of whether a simulation shows strong or weak cooling of the tropical North Atlantic. We find that the high-latitude North Atlantic cooling can directly cool the Indian Ocean through the advection of cold and dry air via the Arabian Sea (Section 3.2.2). The cooling of the Arabian Sea emerges as an important factor driving reduced Indian summer monsoon rainfall (Pausata et al., 2011; Tierney et al., 2015). The relative importance of high-latitude versus tropical mechanisms on Indian summer monsoon rainfall is likely model-dependent (Section 3.2.2). Together, these regions highlight the complexity of regional rainfall responses to weaker AMOC and abrupt cooling of the North Atlantic.

4.3. Responses over the Maritime Continent

An additional challenge is that even the best performing simulations based on their global κ (Fig. 1b) have varying regional responses. Even among the simulations with the highest global model-data agreement (Fig. 1a), the individual rainfall responses in the Amazon, eastern equatorial Africa, and the Maritime Continent do not unambiguously agree with the sign of the ensemble mean rainfall response (Fig. 12). These discrepancies highlight key regions in which future proxy data acquisition and modeling studies may help disentangle competing mechanisms driving the proxy-inferred responses. Furthermore, the Pacific Walker Circulation and the Indian Ocean zonal dipole response to hosing vary among the different simulations (e.g., Fig. 11), making it difficult to assess the role of large atmospheric circulation changes in controlling Maritime Continent rainfall.

4.4. Future directions

Additional high-resolution records from southern Africa, inland Sahel, and southeast Asia would provide additional observational constraints for data sparse regions. Additional climate modeling studies would also further test the proposed mechanisms that explain the regional changes in rainfall. For example, additional sensitivity experiments would help constrain the relative influence of high-latitude versus tropical mechanisms driving the reduction in rainfall over India. The importance of warming of the southern tropical Atlantic could also be refined with further modeling experiments. Recent advances in isotope-enabled modeling may also shed new light on interpreting water isotope proxy records, and understanding the mechanisms driving the proxy-inferred responses in complex regions such as the Maritime Continent (Du et al., 2021), South America (Bao et al., 2023) and the Asian monsoon region (He et al., 2021).

The East Asian monsoon region presents additional complexities. Most simulations show a very weak response in this region (Fig. 1a), but the proxy records, derived primarily from cave speleothem oxygen isotope records (Wang, 2001), show a strong drying signal. One possible explanation for this discrepancy is that the oxygen isotope records from this region may reflect change in the upstream activity along the moisture transport rather than local rainfall amount (Pausata et al., 2011; Liu et al., 2014; Clemens et al., 2010; Hu et al., 2019; He et al., 2021). Due to the longstanding debate about controls on speleothem oxygen isotope values, records from East Asia were excluded from the global kappa analysis in Fig. 1b. In the simulations with full monthly output (Section 2.2), we find a decrease in precipitation in southeastern China, indicating a weakening of the East Asian summer monsoon (Figure S4, JJA). However, there is an increase in precipitation during fall and winter in association with a southward shift of the westerly storm track (Figure S4, SON and DJF), which may explain the inconsistent/weak simulated changes in annual mean precipitation (Figs. 1a and 2). Additional non-isotope high-resolution records and a better understanding of water isotope proxy systems in East Asia are needed to determine the local hydroclimate response in East Asia.

Finally, this work points to other outstanding questions that are good targets for future studies. For example, understanding why some models simulate cooling of the tropical North Atlantic whereas others do not is beyond the scope of this study, but will be an important subject of future work especially given that the magnitude of cooling is not directly related to the amount of freshwater forcing or the reduction in AMOC. In some regions, the southern tropical Atlantic plays an important role in explaining the hydroclimate responses, but it is unclear whether the warming is driven by changes in ocean circulation or atmospheric processes.

5. Conclusion

This study presents a data-model comparison for HS1 to understand the mechanisms of AMOC-driven climate change across the global tropics. Our new proxy data synthesis based on stringent selection criteria and consistent interpretation metrics allows us to identify robust regional hydroclimate signals in the tropics during Heinrich Stadial 1. Using an ensemble of 18 existing and new freshwater hosing simulations, we develop a globally coherent framework to explain how changes in the North Atlantic are transmitted across the global tropics. Specifically, we test whether a previously widely accepted assumption involving a zonally symmetric southward shift of the ITCZ is adequate to explain the observed changes, or if zonally asymmetric mechanisms may play a more important role in certain regions. We find that while both models and data broadly exhibit rainfall patterns consistent with a zonal mean ITCZ shift, this simplistic mechanism fails to fully explain all inferred patterns, particularly outside the Atlantic and in monsoon-sensitive regions. We identify diverse pathways through

which an AMOC reduction propagates across different regions, involving both dynamic and thermodynamic processes. Notably, we highlight the importance of air–sea interactions, including the WES feedback and advection, and large-scale adjustments in global wind patterns. Lastly, we find that simulations with strong to moderate cooling of the tropical North Atlantic generally produce zonally asymmetric rainfall responses that better agree with the proxy data, particularly in the Pacific sector. The disparities among models present crucial areas for future advancements in paleoclimate modeling, in order to enhance our understanding of the dynamical mechanisms underlying changes in rainfall across the global tropics.

CRediT authorship contribution statement

A.E. Lawman: Conceptualization, Methodology, Formal analysis, Investigation, Data curation, Writing – original draft, Writing – review & editing, Visualization, Project administration. **C. Sun:** Conceptualization, Methodology, Formal analysis, Investigation, Data curation, Writing – original draft, Writing – review & editing, Visualization. **X. Wu:** Conceptualization, Methodology, Formal analysis, Investigation, Data curation, Writing – original draft, Writing – review & editing, Visualization. **T. Sun:** Conceptualization, Methodology, Investigation, Data curation, Writing – review & editing. **N. Piatrunia:** Investigation, Data curation, Writing – review & editing. **K. Gomez:** Investigation, Data curation, Writing – review & editing. **M. Kageyama:** Methodology, Investigation, Resources, Writing – review & editing. **U. Merkel:** Methodology, Investigation, Resources, Writing – review & editing. **M. Prange:** Methodology, Investigation, Resources, Writing – review & editing. **B. Otto-Bliesner:** Methodology, Investigation, Resources, Writing – review & editing. **X. Zhang:** Methodology, Investigation, Resources, Writing – review & editing. **P. DiNezio:** Conceptualization, Methodology, Formal analysis, Investigation, Resources, Data curation, Writing – review & editing, Funding acquisition, Supervision. **T. Shanahan:** Conceptualization, Methodology, Formal analysis, Investigation, Resources, Data curation, Writing – review & editing, Funding acquisition, Supervision.

Declaration of competing interest

The authors declare that they have no known competing financial interests or personal relationships that could have appeared to influence the work reported in this paper.

Acknowledgments

This work was supported by the National Science Foundation, United States Grant AGS-2002528 (to P.D.N and T.S.) and the NCAR Advanced Study Program Fellowship (to C. S. and X. W.). M. K. is funded by Centre National de la Recherche Scientifique, France. GENCI (Grand Equipement Natonal de Calcul Intensif) and TGCC (Très Grand Centre du Commissariat à l'Energie Atomique et aux énergies alternatives) are acknowledged for the computing time and resources used to run the IPSL climate model. The LGM simulation has been run in the framework of the Paleoclimate Modelling Intercomparison Project, third phase (https://pmip.lsce.ipsl.fr). U.M. and M.P. were supported by the German Federal Ministry of Education and Science (BMBF) through the "PalMod" project under grant numbers 01LP1915B, 01LP1916C, 01LP2314A, and 01LP2315A. U.M. and M.P. gratefully acknowledge the computing time made available to them on the high performance computers "Lise" and "Emmy" at NHR@ZIB and NHR@Göttingen as part of the NHR infrastructure. B. Otto-Bliesner received support from the NSF National Center for Atmospheric Research (NCAR), which is a major facility sponsored by the National Science Foundation under grant number 1852977. We thank the NOAA National Centers for Environmental Information World Data Service for Paleoclimatology, the PANGAEA Data Publisher for Earth and Environmental Science, and proxy data generators worldwide for making paleoclimate data available to the public. We also acknowledge the Texas Advanced Computing Center for providing the computational resources for generating the CESM1 simulations.

Appendix A. Supplementary data

Supplementary figures S1-S13 referred to in this article can be found online at https://doi.org/10.1016/j.quascirev.2025.109567.

Data availability

The HS1 proxy data synthesis is documented and publicly available via Zenodo (DiNezio et al., 2025a). The multi-model annual mean precipitation and temperature data, and seasonal output for select simulations are available (https://doi.org/10.5281/zenodo.16903147). The NCL, Python, and MATLAB codes used to perform the analyses and generate the figures are available (https://github.com/lawmana/Lawman_etal_2025_QSR/).

References

Baker, P.A., Rigsby, C.A., Seltzer, G.O., Fritz, S.C., Lowenstein, T.K., Bacher, N.P., Veliz, C., 2001. Tropical climate changes at millennial and orbital timescales on the bolivian altiplano. Nature 409 (6821), 698–701. http://dx.doi.org/10.1038/35055524.

Bakker, P., Rogozhina, I., Merkel, U., Prange, M., 2020. Hypersensitivity of glacial summer temperatures in Siberia. Clim. Past 16 (1), 371–386. http://dx.doi.org/10.5194/cp-16-371-2020.

Bao, Y., Liu, Z., He, C., 2023. Dipole response of millennial variability in tropical south American precipitation and $\delta^{18}O_p$ during the last deglaciation. Part I: Rainfall response. J. Clim. 36 (14), 4691–4707. http://dx.doi.org/10.1175/jcli-d-22-0172.1.

Bellomo, K., Angeloni, M., Corti, S., von Hardenberg, J., 2021. Future climate change shaped by inter-model differences in Atlantic meridional overturning circulation response. Nat. Commun. 12 (1), http://dx.doi.org/10.1038/s41467-021-24015-w.

Biasutti, M., Voigt, A., Boos, W.R., Braconnot, P., Hargreaves, J.C., Harrison, S.P., Kang, S.M., Mapes, B.E., Scheff, J., Schumacher, C., Sobel, A.H., Xie, S.-P., 2018. Global energetics and local physics as drivers of past, present and future monsoons. Nat. Geosci. 11 (6), 392–400. http://dx.doi.org/10.1038/s41561-018-0137-1.

Bjerknes, J., 1969. Atmospheric Teleconnections from the equatorial Pacific. Mon. Weather Rev. 97 (3), 163–172. http://dx.doi.org/10.1175/1520-0493(1969)097<0163:atftep>2.3.co;2.

Böhm, E., Lippold, J., Gutjahr, M., Frank, M., Blaser, P., Antz, B., Fohlmeister, J., Frank, N., Andersen, M.B., Deininger, M., 2015. Strong and deep Atlantic meridional overturning circulation during the last glacial cycle. Nature 517 (7532), 73–76. http://dx.doi.org/10.1038/nature14059.

Boos, W.R., Kuang, Z., 2010. Dominant control of the South Asian monsoon by orographic insulation versus plateau heating. Nature 463 (7278), 218–222. http://dx.doi.org/10.1038/nature08707.

Braconnot, P., Otto-Bliesner, B., Harrison, S., Joussaume, S., Peterchmitt, J.Y., Abe-Ouchi, A., Crucifix, M., Driesschaert, E., Fichefet, T., Hewitt, C.D., Kageyama, M., Kitoh, A., Laîné, A., Loutre, M.F., Marti, O., Merkel, U., Ramstein, G., Valdes, P., Weber, S.L., Yu, Y., Zhao, Y., 2007. Results of PMIP2 coupled simulations of the Mid-Holocene and Last Glacial Maximum – Part 1: experiments and large-scale features. Clim. the Past 3 (2), 261–277. http://dx.doi.org/10.5194/cp-3-261-2007.

Bradley, R.S., Diaz, H.F., 2021. Late quaternary abrupt climate change in the tropics and sub-tropics: The continental signal of tropical hydroclimatic events (THEs). Rev. Geophys. 59 (4), http://dx.doi.org/10.1029/2020rg000732.

Broccoli, A.J., Dahl, K.A., Stouffer, R.J., 2006. Response of the ITCZ to Northern Hemisphere cooling. Geophys. Res. Lett. 33 (1), http://dx.doi.org/10.1029/2005gl024546.

Buckley, M.W., Marshall, J., 2016. Observations, inferences, and mechanisms of the Atlantic Meridional Overturning Circulation: A review. Rev. Geophys. 54 (1), 5–63. http://dx.doi.org/10.1002/2015rg000493.

Campos, M.C., Chiessi, C.M., Prange, M., Mulitza, S., Kuhnert, H., Paul, A., Venancio, I.M., Albuquerque, A.L.S., Cruz, F.W., Bahr, A., 2019. A new mechanism for millennial scale positive precipitation anomalies over tropical South America. Quat. Sci. Rev. 225, 105990. http://dx.doi.org/10.1016/j.quascirev.2019.105990.

Chiang, J.C.H., Bitz, C.M., 2005. Influence of high latitude ice cover on the marine Intertropical Convergence Zone. Clim. Dyn. 25 (5), 477–496. http://dx.doi.org/10.1007/s00382-005-0040-5.

Chikamoto, M., Abe-Ouchi, A., Oka, A., Ohgaito, R., Timmermann, A., 2012. Quantifying the ocean's role in glacial CO_2 reductions. Clim. the Past 8 (2), 545–563. http://dx.doi.org/10.5194/cp-8-545-2012.

Chou, C., Neelin, J.D., Su, H., 2001. Ocean-atmosphere-land feedbacks in an idealized monsoon. Q. J. R. Meteorol. Soc. 127 (576), 1869–1891. http://dx.doi.org/10.1002/qj.49712757602.

Clemens, S.C., Prell, W.L., Sun, Y., 2010. Orbital-scale timing and mechanisms driving Late Pleistocene Indo-Asian summer monsoons: Reinterpreting cave speleothem δ^{18}O. Paleoceanography 25 (4), http://dx.doi.org/10.1029/2010PA001926.

Clement, A.C., Peterson, L.C., 2008. Mechanisms of abrupt climate change of the last glacial period. Rev. Geophys. 46 (4), 503–539. http://dx.doi.org/10.1029/2006rg000204.

Cohen, J., 1960. A coefficient of agreement for nominal scales. Educ. Psychol. Meas. 20 (1), 37–46. http://dx.doi.org/10.1177/001316446002000104.

Cook, K.H., 1999. Generation of the african easterly jet and its role in determining west african precipitation. J. Clim. 12 (5), 1165–1184. http://dx.doi.org/10.1175/1520-0442(1999)012<1165:gotaej>2.0.co;2.

Deplazes, G., Lückge, A., Peterson, L.C., Timmermann, A., Hamann, Y., Hughen, K.A., Röhl, U., Laj, C., Cane, M.A., Sigman, D.M., Haug, G.H., 2013. Links between tropical rainfall and North Atlantic climate during the last glacial period. Nature 6 (3), 213–217. http://dx.doi.org/10.1038/ngeo1712.

Deser, C., Phillips, A.S., Tomas, R.A., Okumura, Y.M., Alexander, M.A., Capotondi, A., Scott, J.D., Kwon, Y.-O., Ohba, M., 2012. ENSO and Pacific Decadal Variability in the Community Climate System Model Version 4. J. Clim. 25 (8), 2622–2651. http://dx.doi.org/10.1175/jcli-d-11-00301.1.

DiNezio, Shanahan, T., Sun, T.-Y., Sun, C., Wu, X., Lawman, A., 2025a. Synthesis of hydroclimate changes during Heinrich Stadial 1. http://dx.doi.org/10.5281/zenodo.13881535.

DiNezio, P.N., Shanahan, T.M., Sun, T., Sun, C., Wu, X., Lawman, A., Lea, D., Kageyama, M., Merkel, U., Prange, M., Otto-Bliesner, B., Zhang, X., 2025b. Tropical response to ocean circulation slowdown raises future drought risk. Nature http://dx.doi.org/10.1038/s41586-025-09319-x.

DiNezio, Tierney, J.E., 2013. The effect of sea level on glacial Indo-Pacific climate. Nature 6 (6), 485–491. http://dx.doi.org/10.1038/ngeo1823.

Diongue, A., Lafore, J.-P., Redelsperger, J.-L., Roca, R., 2002. Numerical study of a Sahelian synoptic weather system: Initiation and mature stages of convection and its interactions with the large-scale dynamics. Q. J. R. Meteorol. Soc. 128 (584), 1899–1927. http://dx.doi.org/10.1256/003590002320603467.

Du, X., Russell, J.M., Liu, Z., Otto-Bliesner, B.L., Gao, Y., Zhu, C., Oppo, D.W., Mohtadi, M., Yan, Y., Galy, V.V., He, C., 2021. Deglacial trends in Indo-Pacific warm pool hydroclimate in an isotope-enabled Earth system model and implications for isotope-based paleoclimate reconstructions. Quat. Sci. Rev. 270, 107188. http://dx.doi.org/10.1016/j.quascirev.2021.107188.

Du, X., Russell, J.M., Liu, Z., Otto-Bliesner, B.L., Oppo, D.W., Mohtadi, M., Zhu, C., Galy, V.V., Schefuß, E., Yan, Y., Rosenthal, Y., Dubois, N., Arbuszewski, J., Gao, Y., 2023. North Atlantic cooling triggered a zonal mode over the Indian Ocean during Heinrich Stadial 1. Sci. Adv. 9 (1), http://dx.doi.org/10.1126/sciadv.add4909.

Erokhina, O., Rogozhina, I., Prange, M., Bakker, P., Bernales, J., Paul, A., Schulz, M., 2017. Dependence of slope lapse rate over the greenland ice sheet on background climate. J. Glaciol. 63 (239), 568–572.

Fontaine, B., Garcia-Serrano, J., Roucou, P., Rodriguez-Fonseca, B., Losada, T., Chauvin, F., Gervois, S., Sijikumar, S., Ruti, P., Janicot, S., 2010. Impacts of warm and cold situations in the Mediterranean basins on the West African monsoon: observed connection patterns (1979–2006) and climate simulations. Clim. Dyn. 35 (1), 95–114. http://dx.doi.org/10.1007/s00382-009-0599-3.

Fornace, K.L., Hughen, K.A., Shanahan, T.M., Fritz, S.C., Baker, P.A., Sylva, S.P., 2014. A 60, 000-year record of hydrologic variability in the central andes from the hydrogen isotopic composition of leaf waxes in lake titicaca sediments. Earth Planet. Sci. Lett. 408, 263–271. http://dx.doi.org/10.1016/j.epsl.2014.10.024.

Garreaud, 2009. The andes climate and weather. Adv. Geosci. 22, 3–11. http://dx.doi.org/10.5194/adgeo-22-3-2009, URL http://dx.doi.org/10.5194/adgeo-22-3-2009.

Garreaud, Vuille, M., Clement, A.C., 2003. The climate of the altiplano: observed current conditions and mechanisms of past changes. Palaeogeogr. Palaeoclimatol. Palaeoecol. 194 (1–3), 5–22. http://dx.doi.org/10.1016/s0031-0182(03)00269-4.

He, F., 2011. Simulating transient climate evolution of the last deglaciation with CCSM3. Diss. Univ. Wisconsin- Madison.

He, Liu, Z., Otto-Bliesner, B.L., Brady, E., Zhu, C., Tomas, R., Clark, P., Zhu, J., Jahn, A., Gu, S., Zhang, J., Nusbaumer, J., Noone, D., Cheng, H., Wang, Y., Yan, M., Bao, Y., 2021. Hydroclimate footprint of pan-Asian monsoon water isotope during the last deglaciation. Sci. Adv. 7 (4), http://dx.doi.org/10.1126/sciadv.abe2611.

Hendy, I.L., Kennett, J.P., Roark, E.B., Ingram, B.L., 2002. Apparent synchroneity of submillennial scale climate events between Greenland and Santa Barbara Basin, California from 30–10 ka. Quat. Sci. Rev. 21 (10), 1167–1184. http://dx.doi.org/10.1016/s0277-3791(01)00138-x.

Hu, J., Emile-Geay, J., Tabor, C., Nusbaumer, J., Partin, J., 2019. Deciphering oxygen isotope records from Chinese speleothems with an isotope-enabled climate model. Paleoceanogr. Paleoclimatology 34 (12), 2098–2112. http://dx.doi.org/10.1029/2019pa003741.

Hughen, K.A., Overpeck, J.T., Peterson, L.C., Trumbore, S., 1996. Rapid climate changes in the tropical Atlantic region during the last deglaciation. Nature http://dx.doi.org/10.1038/380051a0.

Kageyama, M., Braconnot, P., Bopp, L., Caubel, A., Foujols, M.-A., Guilyardi, E., Khodri, M., Lloyd, J., Lombard, F., Mariotti, V., Marti, O., Roy, T., Woillez, M.-N., 2012. Mid-Holocene and Last Glacial Maximum climate simulations with the IPSL model—part I: comparing IPSL_CM5A to IPSL_CM4. Clim. Dyn. 40 (9–10), 2447–2468. http://dx.doi.org/10.1007/s00382-012-1488-8.

Kageyama, M., Merkel, U., Otto-Bliesner, B., Prange, M., Abe-Ouchi, A., Lohmann, G., Ohgaito, R., Roche, D., Singarayer, J., Swingedouw, D., Zhang, X., 2013. Climatic impacts of fresh water hosing under Last Glacial Maximum conditions: a multi-model study. Clim. the Past 9 (2), 935–953. http://dx.doi.org/10.5194/cp-9-935-2013.

Kageyama, M., Mignot, J., Swingedouw, D., Marzin, C., Alkama, R., Marti, O., 2009. Glacial climate sensitivity to different states of the Atlantic Meridional Overturning Circulation: results from the IPSL model. Clim. the Past 5 (3), 551–570. http://dx.doi.org/10.5194/cp-5-551-2009.

Kageyama, M., Paul, A., Roche, D.M., Van Meerbeeck, C.J., 2010. Modelling glacial climatic millennial-scale variability related to changes in the Atlantic meridional overturning circulation: a review. Quat. Sci. Rev. 29 (21–22), 2931–2956. http://dx.doi.org/10.1016/j.quascirev.2010.05.029.

Kang, S.M., Held, I.M., Frierson, D.M.W., Zhao, M., 2008. The response of the ITCZ to extratropical thermal forcing: Idealized slab-ocean experiments with a GCM. J. Clim. 21 (14), 3521–3532. http://dx.doi.org/10.1175/2007jcli2146.1.

Kent, C., Chadwick, R., Rowell, D.P., 2015. Understanding uncertainties in future projections of seasonal tropical precipitation. J. Clim. 28 (11), 4390–4413. http://dx.doi.org/10.1175/jcli-d-14-00613.1.

Kienast, S.S., Friedrich, T., Dubois, N., Hill, P.S., Timmermann, A., Mix, A.C., Kienast, M., 2013. Near collapse of the meridional SST gradient in the eastern equatorial Pacific during Heinrich Stadial 1. Paleoceanography 28 (4), 663–674. http://dx.doi.org/10.1002/2013pa002499.

Kilbourne, K.H., Wanamaker, A.D., Moffa-Sanchez, P., Reynolds, D.J., Amrhein, D.E., Butler, P.G., Gebbie, G., Goes, M., Jansen, M.F., Little, C.M., Mette, M., Moreno-Chamarro, E., Ortega, P., Otto-Bliesner, B.L., Rossby, T., Scourse, J., Whitney, N.M., 2022. Atlantic circulation change still uncertain. Nat. Geosci. 15 (3), 165–167.

Lamb, H.F., Bates, C.R., Coombes, P.V., Marshall, M.H., Umer, M., Davies, S.J., Dejen, E., 2007. Late pleistocene desiccation of Lake Tana, source of the blue nile. Quat. Sci. Rev. 26 (3–4), 287–299. http://dx.doi.org/10.1016/j.quascirev.2006.11.020.

Lippold, J., Grützner, J., Winter, D., Lahaye, Y., Mangini, A., Christl, M., 2009. Does sedimentary ^{231}Pa/^{230}Th from the Bermuda Rise monitor past Atlantic Meridional Overturning Circulation? Geophys. Res. Lett. 36 (12), http://dx.doi.org/10.1029/2009gl038068.

Liu, Chiang, J.C.H., Chou, C., Patricola, C.M., 2014. Atmospheric teleconnection mechanisms of extratropical North Atlantic SST influence on Sahel rainfall. Clim. Dyn. 43 (9–10), 2797–2811. http://dx.doi.org/10.1007/s00382-014-2094-8.

Liu, Z., Otto-Bliesner, B.L., He, F., Brady, E.C., Tomas, R., Clark, P.U., Carlson, A.E., Lynch-Stieglitz, J., Curry, W., Brook, E., Erickson, D., Jacob, R., Kutzbach, J., Cheng, J., 2009. Transient simulation of last deglaciation with a new mechanism for Bolling-Allerod warming. Science 325 (5938), 310–314. http://dx.doi.org/10.1126/science.1171041.

Ma, Q., Shi, X., Scholz, P., Sidorenko, D., Lohmann, G., Ionita, M., 2024. Revisiting climate impacts of an AMOC slowdown: dependence on freshwater locations in the North Atlantic. Sci. Adv. 10 (47), http://dx.doi.org/10.1126/sciadv.adr3243.

Manabe, S., Stouffer, R.J., 1995. Simulation of abrupt climate change induced by freshwater input to the North Atlantic Ocean. Nature http://dx.doi.org/10.1038/378165a0.

Marshall, J., Donohoe, A., Ferreira, D., McGee, D., 2013. The ocean's role in setting the mean position of the inter-tropical convergence zone. Clim. Dyn. 42 (7–8), 1967–1979. http://dx.doi.org/10.1007/s00382-013-1767-z.

Marzin, C., Kallel, N., Kageyama, M., Duplessy, J.C., Braconnot, P., 2013. Glacial fluctuations of the Indian monsoon and their relationship with North Atlantic climate: new data and modelling experiments. Clim. the Past 9 (5), 2135–2151. http://dx.doi.org/10.5194/cp-9-2135-2013.

McGee, D., Donohoe, A., Marshall, J., Ferreira, D., 2014. Changes in ITCZ location and cross-equatorial heat transport at the Last Glacial Maximum, Heinrich Stadial 1, and the mid-Holocene. Earth Planet. Sci. Lett. 390 (C), 69–79. http://dx.doi.org/10.1016/j.epsl.2013.12.043.

McGee, D., Moreno-Chamarro, E., Green, B., Marshall, J., Galbraith, E., Bradtmiller, L., 2018. Hemispherically asymmetric trade wind changes as signatures of past ITCZ shifts. Quat. Sci. Rev. 180, 214–228. http://dx.doi.org/10.1016/j.quascirev.2017.11.020.

McManus, J.F., Francois, R., Gherardi, J.-M., Keigwin, L.D., Brown-Leger, S., 2004. Collapse and rapid resumption of atlantic meridional circulation linked to deglacial climate changes. Nature 428 (6985), 834–837. http://dx.doi.org/10.1038/nature02494.

Merkel, U., Prange, M., Schulz, M., 2010. ENSO variability and teleconnections during glacial climates. Quat. Sci. Rev. 29 (1–2), 86–100. http://dx.doi.org/10.1016/j.quascirev.2009.11.006.

Mohr, K.I., Thorncroft, C.D., 2006. Intense convective systems in West Africa and their relationship to the African easterly jet. Q. J. R. Meteorol. Soc. 132 (614), 163–176. http://dx.doi.org/10.1256/qj.05.55.

Mohtadi, M., Prange, M., Oppo, D.W., Pol-Holz, R.D., Merkel, U., Zhang, X., Steinke, S., Lückge, A., 2014. North Atlantic forcing of tropical Indian Ocean climate. Nature 509 (7498), 76–80. http://dx.doi.org/10.1038/nature13196.

Mulitza, S., Prange, M., Stuut, J.-B., Zabel, M., von Dobeneck, T., Itambi, A.C., Nizou, J., Schulz, M., Wefer, G., 2008. Sahel megadroughts triggered by glacial slowdowns of atlantic meridional overturning. Paleoceanography 23 (4), n/a–n/a. http://dx.doi.org/10.1029/2008pa001637.

Neukom, R., Rohrer, M., Calanca, P., Salzmann, N., Huggel, C., Acuña, D., Christie, D.A., Morales, M.S., 2015. Facing unprecedented drying of the Central Andes? Precipitation variability over the period AD 1000–2100. Environ. Res. Lett. 10 (8), 084017. http://dx.doi.org/10.1088/1748-9326/10/8/084017.

Nicholson, S.E., 2008. The intensity, location and structure of the tropical rainbelt over west africa as factors in interannual variability. Int. J. Climatol. 28 (13), 1775–1785. http://dx.doi.org/10.1002/joc.1507.

Nunnery, J.A., Fritz, S.C., Baker, P.A., Salenbien, W., 2018. Lake-level variability in salar de coipasa, bolivia during the past ~40, 000 yr. Quat. Res. 91 (2), 881–891. http://dx.doi.org/10.1017/qua.2018.108.

Orihuela-Pinto, B., England, M.H., Taschetto, A.S., 2022. Interbasin and interhemispheric impacts of a collapsed Atlantic Overturning Circulation. Nat. Clim. Chang. 12 (6), 558–565. http://dx.doi.org/10.1038/s41558-022-01380-y.

Oster, J.L., Macarewich, S., Lofverstrom, M., de Wet, C., Montañez, I., Lora, J.M., Skinner, C., Tabor, C., 2023. North Atlantic meltwater during Heinrich Stadial 1 drives wetter climate with more atmospheric rivers in western North America. Sci. Adv. 9 (46), http://dx.doi.org/10.1126/sciadv.adj2225.

Otto-Bliesner, B.L., Brady, E.C., 2010. The sensitivity of the climate response to the magnitude and location of freshwater forcing: Last Glacial Maximum experiments. Quat. Sci. Rev. 29 (1–2), 56–73. http://dx.doi.org/10.1016/j.quascirev.2009.07.004.

Partin, J.W., Cobb, K.M., Adkins, J.F., Clark, B., Fernandez, D.P., 2007. Millennial-scale trends in west Pacific warm pool hydrology since the Last Glacial Maximum. Nature 449 (7161), 452–455. http://dx.doi.org/10.1038/nature06164.

Pausata, F.S.R., Battisti, D.S., Nisancioglu, K.H., Bitz, C.M., 2011. Chinese stalagmite δ18O controlled by changes in the Indian monsoon during a simulated Heinrich event. Nat. Geosci. 4 (7), 474–480. http://dx.doi.org/10.1038/ngeo1169.

Peterson, L.C., 2000. Rapid Changes in the Hydrologic Cycle of the Tropical Atlantic During the Last Glacial. Science 290 (5498), 1947–1951. http://dx.doi.org/10.1126/science.290.5498.1947.

Placzek, C., Quade, J., Patchett, P.J., 2006. Geochronology and stratigraphy of late pleistocene lake cycles on the southern bolivian altiplano: Implications for causes of tropical climate change. Geol. Soc. Am. Bull. 118 (5–6), 515–532. http://dx.doi.org/10.1130/b25770.1.

Pörtner, H.-O., Roberts, D., Tignor, M., Poloczanska, E., Mintenbeck, K., Alegría, A., Craig, M., Langsdorf, S., Löschke, S., Möller, V., Okem, A., (eds.), B.R., 2022. Climate Change 2022: Impacts, Adaptation and Vulnerability. Contribution of Working Group II to the Sixth Assessment Report of the Intergovernmental Panel on Climate Change. Cambridge University Press, city=Cambridge, UK, p. 3056 pp.. http://dx.doi.org/10.1017/9781009325844.

Ramirez, E., Hoffmann, G., Taupin, J., Francou, B., Ribstein, P., Caillon, N., Ferron, F., Landais, A., Petit, J., Pouyaud, B., Schotterer, U., Simoes, J., Stievenard, M., 2003. A new andean deep ice core from nevado illimani (6350 m), bolivia. Earth Planet. Sci. Lett. 212 (3–4), 337–350. http://dx.doi.org/10.1016/s0012-821x(03)00240-1.

Ravelo, A.C., Hillaire-Marcel, C., 2007. Chapter Eighteen The Use of Oxygen and Carbon Isotopes of Foraminifera in Paleoceanography. In: Proxies in Late Cenozoic Paleoceanography. Elsevier, pp. 735–764.

Schneider, T., Bischoff, T., Haug, G.H., 2014. Migrations and dynamics of the intertropical convergence zone. Nature 513 (7516), 45–53. http://dx.doi.org/10.1038/nature13636.

Singarayer, J.S., Valdes, P.J., 2010. High-latitude climate sensitivity to ice-sheet forcing over the last 120kyr. Quat. Sci. Rev. 29 (1–2), 43–55. http://dx.doi.org/10.1016/j.quascirev.2009.10.011.

Stager, J.C., Ryves, D.B., Chase, B.M., Pausata, F., 2011. Catastrophic drought in the Afro-Asian monsoon region during Heinrich event 1. Science http://dx.doi.org/10.1126/science.1198322.

Stanford, J., Rohling, E., Bacon, S., Roberts, A., Grousset, F., Bolshaw, M., 2011. A new concept for the paleoceanographic evolution of Heinrich event 1 in the North Atlantic. Quat. Sci. Rev. 30 (9–10), 1047–1066. http://dx.doi.org/10.1016/j.quascirev.2011.02.003.

Stouffer, R.J., Yin, J., Gregory, J.M., KW Dixon Journal and 2006 of, 2006. Investigating the causes of the response of the thermohaline circulation to past and future climate changes. J. Clim. 19 (8), 1365–1387. http://dx.doi.org/10.1175/jcli3689.1.

Swingedouw, D., Mignot, J., Braconnot, P., Mosquet, E., Kageyama, M., Alkama, R., 2009. Impact of Freshwater Release in the North Atlantic under Different Climate Conditions in an OAGCM. J. Clim. 22 (23), 6377–6403. http://dx.doi.org/10.1175/2009jcli3028.1.

Sylla, M.B., Coppola, E., Mariotti, L., Giorgi, F., Ruti, P.M., Dell'Aquila, A., Bi, X., 2009. Multiyear simulation of the african climate using a regional climate model (RegCM3) with the high resolution ERA-interim reanalysis. Clim. Dyn. 35 (1), 231–247. http://dx.doi.org/10.1007/s00382-009-0613-9.

Thompson, L., 1998. A 25, 000-year tropical climate history from bolivian ice cores. Science 282 (5395), 1858–1864. http://dx.doi.org/10.1126/science.282.5395.1858.

Tian, B., Dong, X., 2020. The double-ITCZ bias in CMIP3, CMIP5, and CMIP6 models based on annual mean precipitation. Geophys. Res. Lett. 47 (8), http://dx.doi.org/10.1029/2020gl087232.

Tierney, J.E., Pausata, F.S.R., deMenocal, P., 2015. Deglacial Indian monsoon failure and North Atlantic stadials linked by Indian Ocean surface cooling. Nat. Geosci. 9 (1), 46–50. http://dx.doi.org/10.1038/ngeo2603.

Timmermann, A., Okumura, Y., An, S.-I., Clement, A., Dong, B., Guilyardi, E., Hu, A., Jungclaus, J., Renold, M., Stocker, T.F., et al., 2007. The influence of a weakening of the Atlantic meridional overturning circulation on ENSO. J. Clim. 20 (19), 4899–4919. http://dx.doi.org/10.1175/jcli4283.1.

Vellinga, M., Wood, R.A., 2002. Clim. Change 54 (3), 251–267. http://dx.doi.org/10.1023/a:1016168827653.

Vuille, M., Bradley, R.S., 2000. Mean annual temperature trends and their vertical structure in the tropical Andes. Geophys. Res. Lett. 27 (23), 3885–3888. http://dx.doi.org/10.1029/2000gl011871.

Wang, 2001. A high-resolution absolute-dated late pleistocene monsoon record from Hulu Cave, China. Science 294 (5550), 2345–2348. http://dx.doi.org/10.1126/science.1064618.

Wang, X., Auler, A.S., Edwards, R.L., Cheng, H., Cristalli, P.S., Smart, P.L., Richards, D.A., Shen, C.-C., 2004. Wet periods in northeastern Brazil over the past 210 kyr linked to distant climate anomalies. Nature 432 (7018), 740–743. http://dx.doi.org/10.1038/nature03067.

Wang, X., Auler, A.S., Edwards, R.L., Cheng, H., Ito, E., Solheid, M., 2006. Interhemispheric anti-phasing of rainfall during the last glacial period. Quat. Sci. Rev. 25 (23–24), 3391–3403. http://dx.doi.org/10.1016/j.quascirev.2006.02.009.

Wang, Cheng, H., Edwards, R.L., An, Z.S., Wu, J.Y., Shen, C.C., Dorale, J.A., 2001. A high-resolution absolute-dated Late Pleistocene monsoon record from Hulu Cave, China. Science 294 (5550), 2345–2348.

Wang, Y., Cheng, H., Edwards, R.L., Kong, X., Shao, X., Chen, S., Wu, J., Jiang, X., Wang, X., An, Z., 2008. Millennial- and orbital-scale changes in the East Asian monsoon over the past 224,000 years. Nature 451 (7182), 1090–1093. http://dx.doi.org/10.1038/nature06692.

Wen, C., Chang, P., Saravanan, R., 2011. Effect of Atlantic Meridional Overturning Circulation on tropical Atlantic variability: A regional coupled model study. J. Clim. 24 (13), 3323–3343. http://dx.doi.org/10.1175/2011jcli3845.1.

Xie, S.-P., Okumura, Y., Miyama, T., Timmermann, A., 2008. Influences of Atlantic climate change on the tropical Pacific via the Central American Isthmus. J. Clim. 21 (15), 3914–3928. http://dx.doi.org/10.1175/2008jcli2231.1.

Xie, S.-P., Philander, S.G.H., 1994. A coupled ocean-atmosphere model of relevance to the ITCZ in the eastern Pacific. Tellus A 46 (4), 340–350. http://dx.doi.org/10.3402/tellusa.v46i4.15484.

Zhang, Delworth, T.L., 2005. Simulated tropical response to a substantial weakening of the Atlantic thermohaline circulation. J. Clim. 18 (12), 1853–1860. http://dx.doi.org/10.1175/jcli3460.1.

Zhang, X., Lohmann, G., Knorr, G., Xu, X., 2013. Different ocean states and transient characteristics in Last Glacial Maximum simulations and implications for deglaciation. Clim. Past 9 (5), 2319–2333. http://dx.doi.org/10.5194/cp-9-2319-2013.